Doctoral Dissertation (Shinshu University)

Metallophthalocyanine analogues fused with polycyclic aromatics and their optoelectronic functions

-March 2016-

Hiroyuki SUZUKI

CONTENTS

Chapter 1

General introduction

Chapter 2

Self-organized one-dimensional columns of benzo[*b*]thiophene-fused tetraazaporphyrins

Chapter 3

Topological control of columnar stacking made of liquid-crystalline thiophene-fused metallonaphthalocyanines

Chapter 4

Supramolecular complex formation of resorcin [4]arene-modified zinc phthalocyanine and fullerene

Abbreviations

AFM	Atomic force microscope
C_{60}	fullerene
Col_r	Rectangular columnar
DBU	1,8-Diazabicyclo[5.4.0]-7-undecene
DFT	Density functional theory
DSC	Differential scanning calorimetry
HOMO	Highest occupied molecular orbital
HPLC	High performance liquid chromatography
ITO	Indium tin oxide
IR	Infrared
LUMO	Lowest occupied molecular orbital
MALDI	Matrix assisted laser deposition/ionization
MPc	Metallophthalocyanine
Nc	Naphthalocyanines
NMR	Nuclear magnetic resonance
OFET	Organic field effect transistor
Pc	Phthalocyanine
S-Phos	2-Dicyclohexylphosphino-2'.6'-dimethoxybiphenyl
TGA	Thermo gravimetric analysis
THF	Tetrahydrofuran
TOF	Time of flight
TPOM	Temperature-controlled polarized microscope
UV-Vis	Ultraviolet-visible
XRD	X-ray diffraction
π-A	The surface pressure versus area

List of Figures

Chapter 1

Chapter 2

Chapter 3

Chapter 4

Chapter 1

General introduction

Concept

The systematically exploring of molecular structures and control of molecular orientation generate superior molecular functions. In this thesis, the author has focused on molecular functions of two-dimensional (2D) π-conjugated molecular materials. The expansion of conjugation allows a delocalization of π electrons across all the adjacent aligned π-orbitals, and may lower the overall energy of the molecules.[1] Recently, there is growing interest in developing conjugated molecules possessing two or three dimensional conjugation.[2] The extension of π-electron delocalization showed various unique properties, including high mobility and variable band-gap, and can alter intermolecular interactions among molecules. The author developed several bottom-up synthetic routes for 2D conjugated molecules containing heteroatoms and metal ions, and investigated the structural effects of 2D molecules on their electronic and photonic properties.

1.1 Polycyclic Aromatics

Graphene has been regarded as an attractive material since it was discovered by Geim and Novoselv *et al.* in 2004, and has drawn enormous interest among researchers as a result of its intrinsic electronic and magnetic properties.[3-6] Polycyclic aromatic hydrocarbons (PAHs), which make up graphene segments, have large π-conjugated systems. Following the synthetic break-through of hexa-*peri*-hexabenzocoronene (*p*-HBC) by Müllen *et al*. in 1995, impressive progress has been achieved, and more complex PAHs with different shapes and sizes have been reported; for example, a giant molecular graphene containing 222 carbon atoms with a disk diameter of 3.2 nm.[7,8]

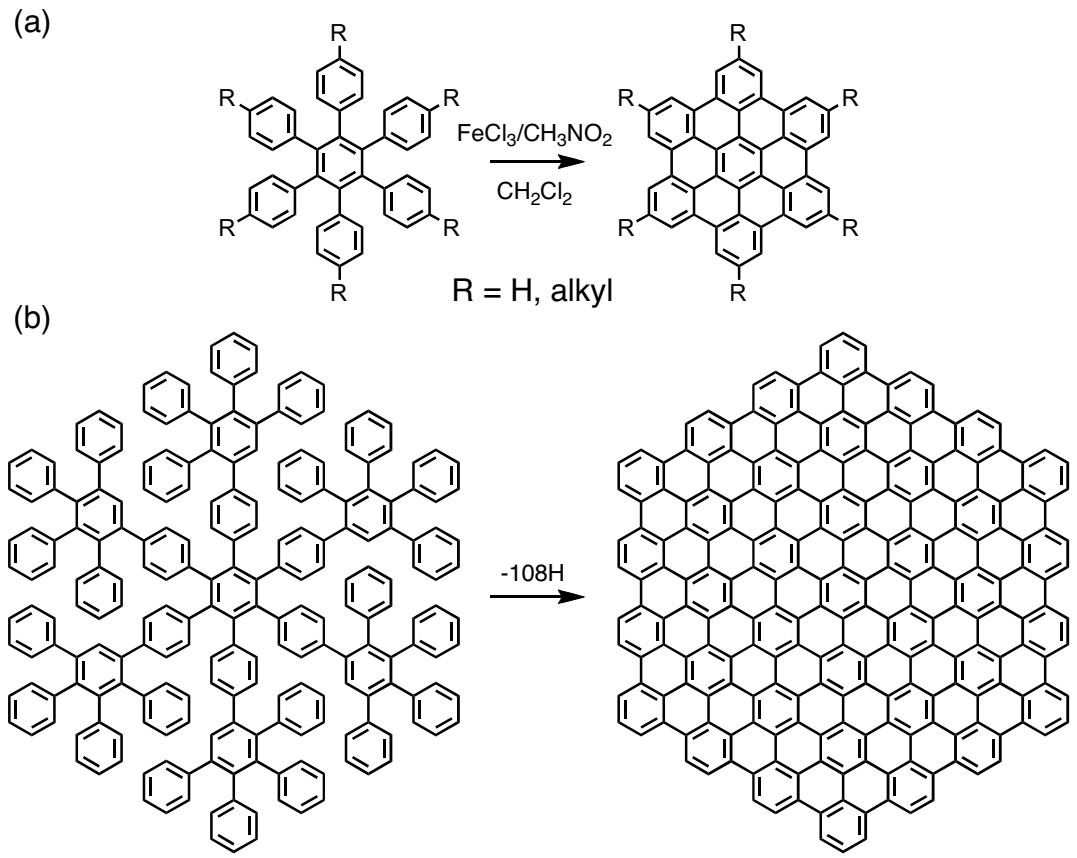

***Fig. 1**. a) Route to p-HBC. b) Example of giant molecular graphene.*

In the last decade, the extended PAHs have thus attracted renewed organic synthetic interest and more academic attention as structurally well-defined graphenoid molecules with great potential in future applications, such as in nanoelectronics, optoelectronics and spintronics.[9-14] In particular, *p*-HBC is a typical graphene fragment with a planar disk-shaped structure and displays remarkable performance in liquid crystalline materials because of its strong intermolecular π-π interactions and highly ordered columnar packing.[15-17]

Recently, this large body of work inspired new research directions, such as studies focussed on *cata*-fused HBC isomers (*c*-HBC) and large heterocyclic aromatic hydrocarbons (H-PAHs). Nuckolls *et al*. reported the parent *c*-HBC and a variety of its substituted derivatives, and disclosed their unique nonplanar structure and intriguing electronic and self-assembly properties, such as their strong tendency to self-assemble into nanowires and nanotube, and to form shape-complementary complexes with C_{60}.[14-18]

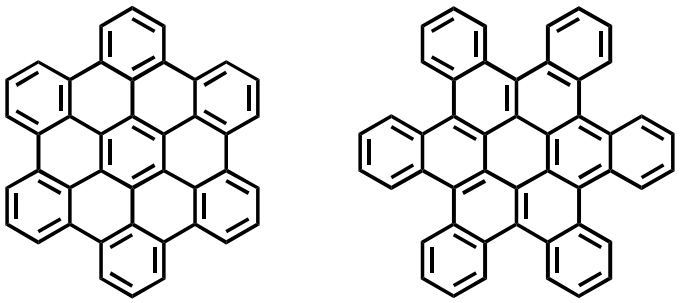

***Fig. 2**. Structure of HBC isomers.*

H-PAHs are a new class of materials that possess properties and functions different from those of the parent PAHs. Among these, thiophene-fused PAHs have been extensively explored due to their wide-ranging applications in organic electronic devices.[19,20] In 2007, Müllen *et al*. synthesized a tribenzothiophene-fused

p-HBC as the first example of this type of molecule with embedded thiophene rings.[21] In addition, Nuckolls *et al*. developed a synthesis of dibenzotetrathienocoronene (DBTTC), a thiophene-fused *c*-HBC analogue.[22,23] The aromatic core of DBTTC could self-assemble into a columnar superstructure, which merged into a three-dimensional network of supramolecular cables. When the acceptor C_{60} was evaporated onto this network, a nanostructured p–n bulk heterojunction was formed, providing a power conversion efficiency (PCE) of 1.9% in a solar cell device. Furthermore, solution-processed photovoltaic devices of DBTTC and phenyl-C_{70}-butyric acid methyl ester ($PC_{70}BM$) showed a PCE of 2.7%, where a supramolecular complex between DBTTC and $PC_{70}BM$ was demonstrated to play an important role in the charge separation process.[24]

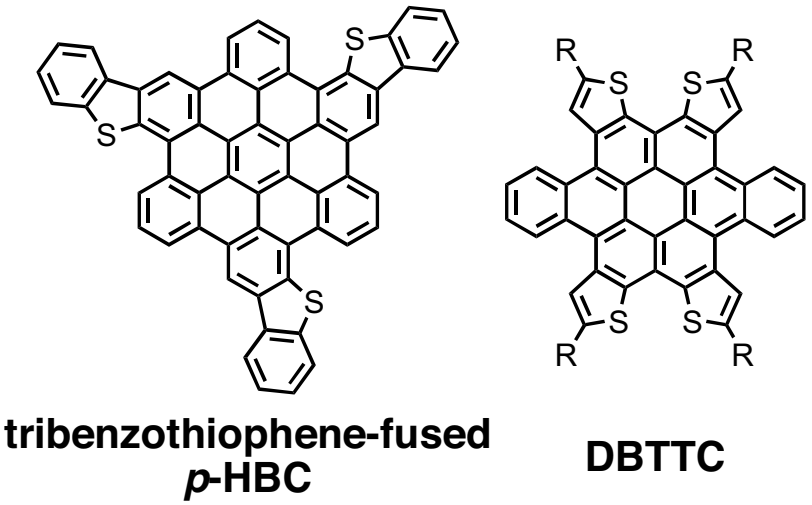

Fig. 3. *Example of thiophene-fused PAHs*

1.2 Phthalocyanines

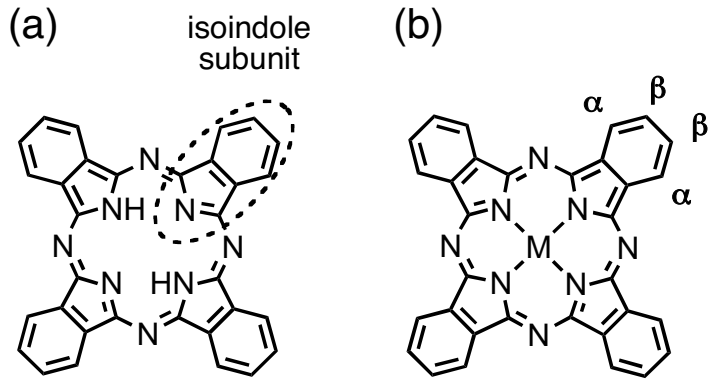

***Fig. 4**. a) Metal-free phthalocyanine. b) Metallophthalocyanines.*

Phthalocyanine

Phthalocyanines (Pcs) are porphyrin analogues composed of four isoindole subunits linked together through nitrogen atoms. The name "phthalocyanine" was first used by Linstead in 1933 to describe a class of organic dyes whose colors range from blue to green.[25] Papers reported by Linstead contained the experimental details for the preparation of Pcs from phthalonitrile (*o*-dicyanobenzene), which is still considered the best precursor for Pc synthesis on a laboratory scale. Currently, the two hydrogen atoms in the center of the molecule can be replaced by more than 70 different elements, including virtually all the metals in the periodic table, forming various types of metallophthalocyanine (MPc).

Almost all the early Pcs were unsubstituted on the periphery of the core structure and had high insolubility in most known solvents, even in high-boiling aromatic solvents such as 1-chloro- or 1-bromonaphthalene and quinoline, whereas sulfuric acid was found to be the best solvent. To increase the solubility of Pcs in common organic solvents, a great variety of substituents can be introduced into the periphery (α- and β-positions) of the macrocycle. Furthermore, this also permits the

electronic structure of the system to be altered, which can be used for an accurate tuning of optical, redox, and organizational properties of Pcs. Therefore, the chemical flexibility, good environmental stability, as well as electrical and photochemical properties of this class of compound allow the preparation of a large variety of unique derivatives for an incredible number of applications, including organic solar cells, field effect transistors, nonlinear optics, high dielectric materials, electrochromic devices, photodynamic therapy (PDT), and chemical sensors.[26-32]

Character of phthalocyanine

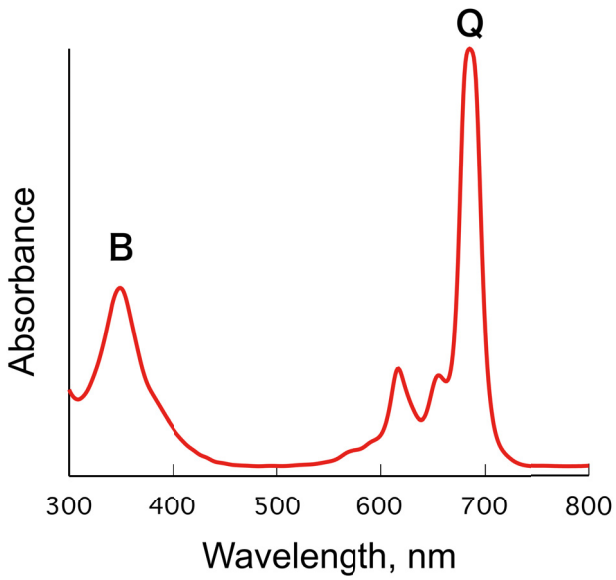

Fig. 5*. UV-Vis spectrum of MPcs in THF.*

MPcs are the most commercially important material of porphyrazine analogues because of the intense π-π* transitions from doubly-degenerate orbitals in the visible region. The main and most characteristic feature of the electronic absorption spectra of MPcs is the presence of two very intensive bands, the Q-band and the Soret or B-band. Due to their 18 π-electron conjugated chromophore system, MPcs

exhibit high extinction coefficients of approximately 10^5 $M^{-1}cm^{-1}$. The Q band is usually found in the region of 650-730 nm, and is responsible for the green or blue color of these compounds. This single main band is associated with transitions from the highest occupied molecular orbital (HOMO) to the lowest unoccupied molecular orbital (LUMO). In the case of MPcs, having D_{4h} symmetry, the LUMO is degenerate, and only one band is observed. In contrast, the Q-band of metal-free Pcs is split, due to their D_{2h} symmetry. Consequently, the LUMO orbital loses degeneracy, giving rise to Qx and Qy states. Interestingly, it was found that the oscillator strength of the Q band of the MPcs is about twice that of the metal-free absorbance band. The Soret band is situated at higher energies in the spectrum, and is related to π-π* transitions from lower-energy molecular orbitals.

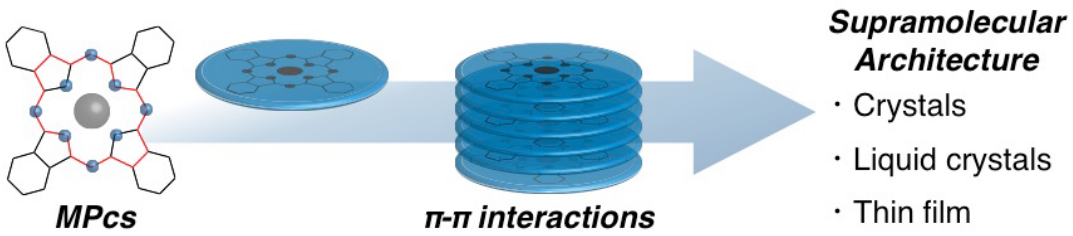

***Fig. 6**. Schematic illustrations of self-organized MPcs.*

Pc molecules exhibit a natural tendency to aggregate through strong π-π interactions between Pc macrocycles, which assist in the formation of multiple and highly ordered condensed phases, such as crystals, liquid crystals, and thin films by using a suitable choice of substituents and central element. In many cases, the type of supramolecular architecture formed can be predicted, and it will determine the final properties and applications of the material.[33,34]

1.3 Ring-expanded Phthalocyanine analogues

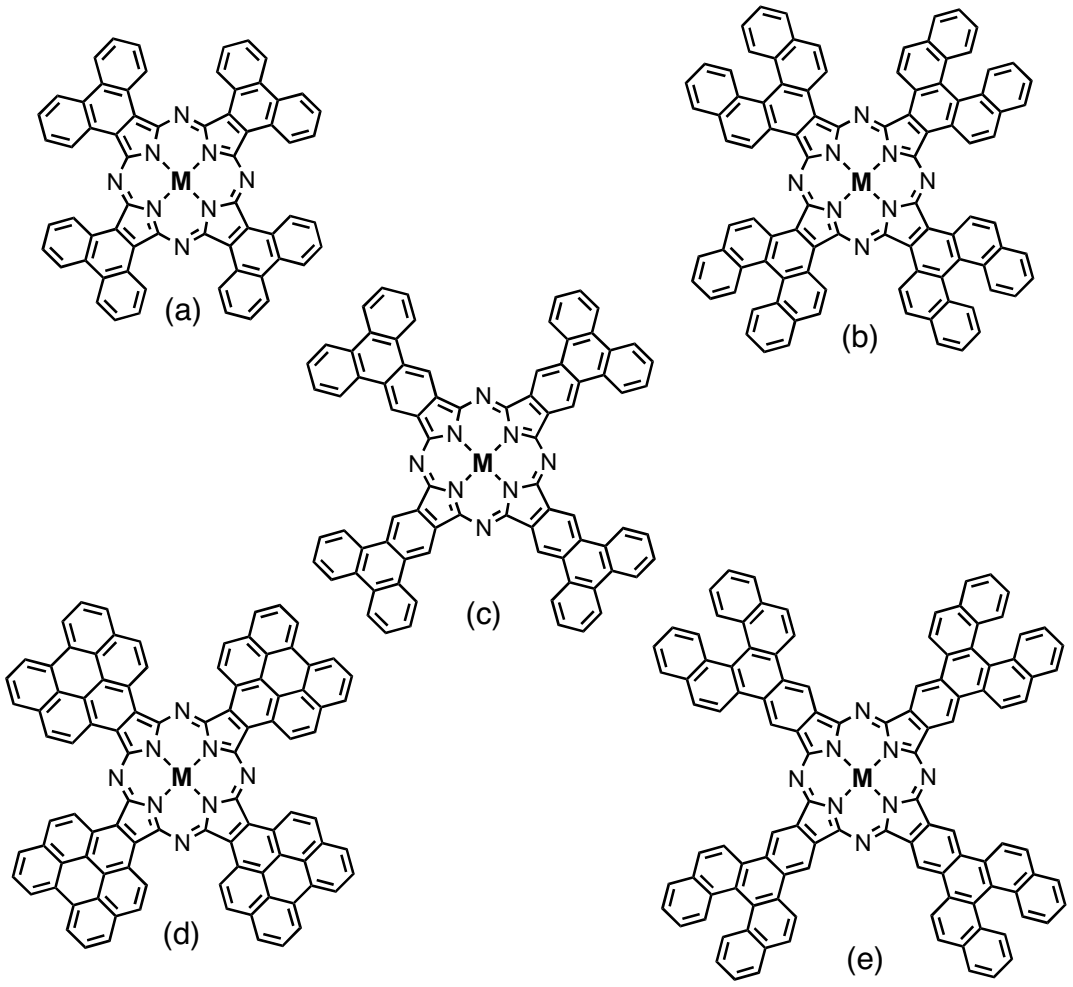

***Fig.** 7. Ring-expanded phthalocyanine analogues: a) Phenanthralocyanine; b) Helicenocyanine; c) Triphenylenophthalocyanine; d) Perylenophthalocyanine; e) Benzohelicenocyanine.*

Ring-expanded phthalocyanine analogues

The electronic properties of core motifs strongly depend on the extent of π-conjugation, and increasing the size of the π system is advantageous in many potential applications. More precisely, extension of the conjugated system, thereby increasing the π-conjugation, continuously destabilizes the HOMO level and shifts

the absorption to longer wavelengths. In addition to the influence on the HOMO–LUMO gap, larger aromatic residues increase the tendency for π-stacking, and hence, aggregation.

Pcs are important molecular materials because of the potential for these types of molecule to form the functional component of optoelectronic devices. Their use in such applications typically requires a combination of molecular (e.g. optical absorption/band gap, redox) and bulk (e.g. processability, self-assembly, mesophase formation) properties. Pc itself can be modified extensively to tune both molecular and bulk properties. The extended π system so-produced allows tuning of the molecular properties, and careful choice of derivative also permits their processing (solubility) and self-assembly (mesophase) properties.

The synthesis of Pcs with extended π-systems is commonly achieved by using an *o*-dicyano precursor for the cyclotetramerization reaction to the Pc.[35-39] Due to a lack of methods for the direct *o*-functionalization of PAHs, precursors were built from long synthetic pathways. To overcome solubility problems, synthetic routes to multiply benzannulated Pcs have been designed to include solubilizing alkyl chains. Considering these three requirements (*o*-dicyano function, short synthesis from large PAH precursors, and solubilizing alkyl chains), new methods are required for the convenient synthesis of new core-extended Pcs.

1.4 Purpose of research

Because structurally well-defined graphenoid molecules have a great potential in future applications, the extended PAHs have attracted renewed organic synthetic interest and more academic attention as structurally interesting species.

In addition, the major approaches for the structural modification of Pcs include: (1) coordination with elements ranging from main group to transition metals via the central nitrogen atoms; (2) introduction of substituents with electron donating or withdrawing effects onto the α- and/or β-positions; and (3) extension of the π-system conjugation using fused aromatic rings. Due to the versatility of chemical synthesis, various Pc-based materials with desired electronic and structural features have been developed.

In this thesis, the author has focused on the design and syntheses of ring-expanded MPc analogues fused with polycyclic aromatics. To control the optical, electronic, and organizational properties of the developed materials, the author synthesized new materials by means of various ring-closure reactions, and then investigated the relationships between molecular structure and characteristic features.

1.5 References

1. Okano S and Tománek D. *Phys. Rev. B*, 2007; **75**: 195409.
2. Yorimitsu H and Bhanuchandra M. *J. Phys. Soc. Jpn*, 2015; **84**: 121016.
3. Novoselov KS, Geim AK, Morozov SV, Jiang D, Zhang Y, Dubonos SV, Grigorieva IV and Firsov AA. *Science* 2004; **306**: 666.
4. Geim AK and Novoselov KS. *Nat. Mater*. 2007; **6**: 183.
5. Service RF. *Science* 2009; **324**: 875.
6. Novoselov KS, Falko VI, Colombo L, Gellert PR, Schwab MG and Kim K. *Nature* 2012; **490**: 192.
7. Watson W, Frechtenkötter A and Müllen K. *Chem. Rev*. 2001; **101**: 1267.
8. Wu J, Pisula W and Müllen K. *Chem. Rev*, 2007; **107**: 718.
9. Yan X and. Li L.-s. *J. Mater. Chem*. 2011; **21**: 3295.
10. Baldridge KK and Siegel JS. *Angew. Chem. Int. Ed*. 2013; **52**: 5436.
11. Pisula W, Feng XL and Müllen K. *Chem. Mater*. 2011; **23**: 554.
12. Morita Y, Suzuki S, Sato K and Takui T. *Nat. Chem*. 2011; **3**: 197.
13. Sun Z, Zeng Z and Wu J. *Chem. – Asian J*. 2013; **8**: 2894.
14. Ball M, Zhong Y, Wu Y, Schenck C, Ng F, Steigerwald M, Xiao S and Nuckolls C. *Acc. Chem. Res*. 2015; **48**: 267.
15. Hill JP, Jin W, Kosaka A, Fukushima T, Ichihara H, Shimomura T, Ito K, Hashizume T, Ishii N and Aida T. *Science* 2004; **304**: 1481
16. Sergeyev S, Pisula W and Geerts YH. *Chem. Soc. Rev*. 2007; **36**: 1902.
17. Pisula W; Feng X and Müllen K. *Adv. Mater*. 2010; **22**: 3634.
18. Tremblay NJ, Gorodetsky AA, Cox MP, Schiros T, Kim B, Steiner R, Bullard Z, Sattler A. So W-Y, Itoh Y, Toney MF, Ogasawara H, Ramirez AP, Kymissis I, Steigerwald ML and Nuckolls C. *ChemPhysChem* 2010; **11**: 799.
19. Takimiya K, Osaka I, Mori T and Nakano M. *Acc. Chem. Res*. 2014; **47**: 1493.
20. Cinar ME and Ozturk T. *Chem. Rev*. 2015; **115**: 3036.
21. Feng X, Wu J, Ai M, Pisula W, Zhi L, Rabe JP and Müllen K. *Angew. Chem. Int. Ed*. 2007; **46**: 3033.

22. Gorodetsky AA, Chiu C.-Y, Schiros T, Palma M, Cox M, Jia Z, Sattler W, Kymissis I, Steigerwald M and Nuckolls C. *Angew. Chem. Int. Ed.* 2010; **49**: 7909.
23. Chiu C-Y, Kim B, Gorodetsky AA, Sattler W, Wei S, Sattler A, Steigerwald M and Nuckolls C. *Chem. Sci.* 2011; **2**: 1480.
24. Kang SJ, Kim JB, Chiu C-Y, Ahn S, Schiros T, Lee SS, Yager KG, Toney MF, Loo Y-L and Nuckolls. *Angew. Chem. Int. Ed.* 2012; **51**: 8594.
25. Linstead RP. *Br. Assoc. Adv. Sci. Rep*1933: 465.
26. Tang CW. *Appl. Phys. Lett.* 1986; **48**: 183.
27. Li L, Tang Q, Li H, Yang X, Hu W, Song Y, Shuai Z, Xu W, Liu Y and Zhu D. *Adv. Mater.* 2007; **19**: 2613.
28. Chen Y, El-Khouly ME, Doyle JJ, Lin Y, Liu Y, Notaras EGA, Blau WJ and O'Flaherty SM. Handb. *Org. Electron. Photonics* 2008; **2**: 151.
29. Opris DM, Nueesch F, Loewe C, Molberg M and Nagel M. *Chem. Mater.* 2008; **20**: 6889.
30. Somani PR and Radhakrishnan S. *Mater. Chem. Phys.* 2003; **77**: 117.
31. Sokolova NV, Schotten T, Berthold HJ, Thiem J and Nenajdenko VG. *Synthesis-Stuttgart* 2013; **45**: 556.
32. Valli L. *Adv. Colloid Interface Sci.* 2005; **116**: 13.
33. van Nostrum CF and Nolte RJM. *Chem. Comm.* 1996; 2385
34. Engelkamp H, Middelbeek S and Nolte RJM. *Science* 1999; **284**: 785.
35. Maya EM, Snow AW, Shirk JS, Flom SR, Pong RGS and Callahan JH. *J. Porphyrins Phthalocyanines* 2002; **6**: 463.
36. Cammidge AN and Gopee H. *Chem. Commun.* 2002; 966.
37. Mandal BK, Sooksimuang T, Lee CH and Wang R. *J. Porphyrins Phthalocyanines* 2006; **10**: 140.
38. Sooksimuang T and Mandal BK. *J. Org. Chem.* 2003; **68**: 652.
39. Cammidge AN and Gopee H. *Chem. Eur. J.* 2006; **12**: 8609.

Chapter 2

Self-organized one-dimensional columns of benzo[*b*]thiophene-fused tetraazaporphyrins

Abstract

Ring-expanded metallophthalocyanines fused with thiophene rings **1**–**4** have been synthesized by ring closing reaction from the *o*-chloroethynylbenzene substructures with Na_2S $9H_2O$. The self-organizing properties of these compounds have been studied by UV-vis spectroscopy in solution, π-A isotherms at air-water interface, X-ray diffraction (XRD) patterns of a solid, and atomic force microscopy (AFM). Whereas all compounds exhibit good solubility in organic solvents, thiophene-fused phthalocyanines form stable aggregates through strong intermolecular π–π interaction. Copper phthalocynaine Cu-**2** possessing phenyl spacers produced long nano-fibrous assemblies from solution.

2.1 Introduction

Large-area and flexible electronic devices fabricated by simple printing technologies using solution-based semiconducting materials have recently been attracting much intense attention due to their potential applications such as flexible displays, smart labels, and light-weight solar cells.[1–6] Various organic and inorganic semiconducting materials have been applied as functional inks for printed electronics. Among these semiconducting materials, well-defined thiophene-fused polycyclic aromatic derivatives with solubilizing groups exhibited excellent performance for organic-based electronic devices.[7] Takimiya *et al.* succeeded at systematic syntheses of solution-processable thiophene-fused aromatic derivatives. Solution-processed organic field-effect transistors (OFETs) fabricated by using solution-cast films of these materials have shown high field-effect mobility values above 1 cm^2 V^{-1} s^{-1}.[8-11] The molecular design of solution-processable organic semiconducting molecules requires long-range intermolecular orbital overlap in the solid state as well as high solubility in solution.

Phthalocyanines (Pcs) and their metal complexes (MPcs) have been used as molecular components in organic-based devices due to their intense absorbing Q-bands (600–700 nm), high molar extinction coefficients ($\varepsilon > 100{,}000$ M^{-1} cm^{-1}), and good thermal, chemical, and photochemical stabilities.[12] Extended flat hydrophobic Pc ligands, modified at either four or eight positions on each Pc with solubilizing side chains, can self-organize to form one-dimensional columns through intermolecular π–π stacking interactions.[12] The π–π overlap of MPcs within the columnar stacks provides a transport pathway for charge or energy parallel to the columnar axis. The long-range transportation of charge and energy in the columnar stacks can enhance the device performance of organic-based optical and electronic devices. The length of self-organized columns depends on the

strength of intermolecular π–π stacking interactions among MPcs. In this context, many attempts have been made to control self-organization properties of MPcs by exploring molecular architecture of Pc ligand.[13-18]

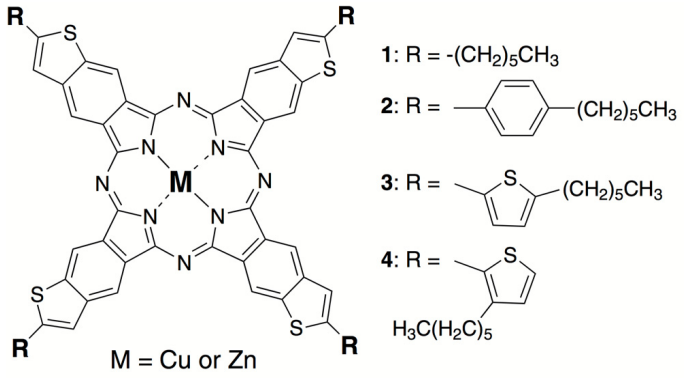

Fig. 1. *Structure of thiophene-fused MPcs* ***1–4****. The structure is one of structural isomers*.

This chapter reports syntheses of thiophene-fused MPc derivatives **1**-**4** through a ring closing reaction from the *o*-chloroethynylbenzene substructures, and their self-organizing properties of ring-expanded MPcs in solution and a solid state (Fig. 1). Although several thiophene-fused tetraazaporphyrins have been synthesized, a benzothiophene-fused teteraazaporphyrin has not been reported.[19-21] The introduction of four peripheral alkyl chains with ring-expanded MPcs exhibits high solubility in organic solvents. Thiophene-fused Cu-**2** decorated with *n*-hexylphenyl substituents formed long fibrous aggregates through enhanced π–π interaction among ring-expanded MPcs. The author also reports preliminary results of the fabrication of OFETs using spin-coated thin films of Cu-**1** and Cu-**2** and the preparation of insoluble Pc-networked film by the electrochemical polymerization of Cu-**4**.

2.2 Experimental section

2.2.1 General procedures

NMR spectra were recorded on a Bruker AVANCE 400 FT NMR spectrometer at 399.65 MHz and 100.62 MHz for ^{1}H and ^{13}C in $CDCl_3$ solution. Chemical shifts are reported relative to internal TMS. IR spectra were obtained on a SHIMAZU IR Prestige-21 with DuraSample IR II. UV-vis spectra were measured on a JASCO V-650. MALDI-TOF mass spectra were obtained on a Bruker autoflex spectrometer with dithranol as matrix.

All chemicals were purchased from commercial suppliers and used without purification. Column chromatography was performed with activated alumina (Wako, 200 mesh) or silica gel (Wakogel C-200). Recycling preparative gel permeation chromatography was carried out by a JAI recycling preparative HPLC using $CHCl_3$ as an eluent. Analytical thin layer chromatography was performed with commercial Merck plates coated with silica gel 60 F_{254} or aluminum oxide 60 F_{254}.

The transition temperatures were measured by differential scanning calorimetry with a SII DSC 6200 operated at a scanning rate of 10 ºC min^{-1} on heating and cooling. The apparatus was calibrated with indium as standard. The XRD patterns were obtained with a Rigaku XRD-DSC with Cu Kα radiation. Spacings were obtained from Bragg's law. Atomic force microscopy images were acquired in non-contact mode by a JEOL JSPM-5400 system.

2.2.2 Syntheses

Phthalonitriles

5. To a solution of 4,5-dichlorophthalonitrile (0.60 g, 3.05 mmol) and 1-octyne

(0.50 g, 4.56 mmol) in triethylamine (4.0 mL) and THF (2.0 mL) were added $PdCl_2(PPh_3)_2$ (64 mg, 0.91 mmol) and Cu(I) (17 mg, 0.90 mmol). The reaction mixture was heated at 80 ºC for 12 h under N_2 atmosphere. After cooling to room temperature, the reaction mixture was poured into water and extracted with CH_2Cl_2. The organic layer was dried over $MgSO_4$ and the solvent was evaporated. The residues was purified by column chromatography on silica gel by eluting with CH_2Cl_2 and *n*-hexane (1:1 v/v) and recycling preparative HPLC to give **5** (0.39 g, 47%). ^{1}H NMR ($CDCl_3$, 400.13 MHz): δ, ppm 7.82 (1H, s, ArH), 7.80 (1H, s, ArH), 2.53 (2H, t, *J* = 7.2 Hz, –CH_2–), 1.62–1.69 (2H, m, –CH_2–), 1.46–1.52 (2H, m, –CH_2–), 1.31–1.35 (4H, m, –CH_2–), 0.90 (3H, t, *J* = 7.2 Hz, –CH_3). ^{13}C NMR ($CDCl_3$, 100.61 MHz): δ, ppm 141.6, 137.7, 134.3, 130.4, 114.8, 114.7, 114.6, 114.4, 105.6, 75.9, 31.6, 28.9, 28.4, 22.9, 20.2, 14.4. IR (ATR): ν, cm^{-1} 2230 (–CN).

6. Compound **6** was synthesized from 4,5-dichlorophthalonitrile and 1-ethynyl-4-hexylbenzene by the same procedure as for **5**. Yield 52%. ^{1}H NMR ($CDCl_3$, 400.13 MHz): δ, ppm 7.91 (1H, s, ArH), 7.83 (1H, s, ArH), 7.49 (2H, d, *J* = 8.4 Hz, ArH), 7.22 (2H, d, *J* = 8.4 Hz, ArH), 2.65 (2H, t, *J* = 7.6 Hz, –CH_2–), 1.58–1.66 (2H, m, –CH_2–), 1.28–1.35 (6H, m, –CH_2–), 0.89 (3H, t, *J* = 6.8 Hz, –CH_3). ^{13}C NMR ($CDCl_3$, 100.61 MHz): δ, ppm 146.4, 141.3, 137.4, 134.4, 132.5, 130.0, 129.3, 118.5, 115.0, 114.7, 114.6, 114.5, 103.1, 83.5, 36.5, 32.1, 31.5, 29.3, 23.0, 14.5. IR (ATR): ν, cm^{-1} 2230 (–CN).

7. Compound **7** was synthesized from 4,5-dichlorophthalonitrile and 2-ethynyl-5-hexylthiophene by the same procedure as for **5**. Yield 42%. ^{1}H NMR ($CDCl_3$, 400.13 MHz): δ, ppm 7.88 (1H, s, ArH), 7.83 (1H, s, ArH), 7.27 (1H, d, *J* = 3.6 Hz, ArH), 6.76 (1H, d, *J* = 3.6 Hz, ArH), 2.84 (2H, t, *J* = 7.6 Hz, –CH_2–), 1.65–1.73 (2H, m, –CH_2–), 1.29–1.40 (6H, m, –CH_2–), 0.89 (3H, t, *J* = 6.8 Hz, –CH_3). ^{13}C NMR ($CDCl_3$, 100.61 MHz): δ, ppm 152.7, 140.6, 136.8, 135.4, 134.3, 129.8, 125.5, 118.3, 114.7, 114.6, 114.5, 96.9, 87.4, 31.9, 31.3, 30.8, 29.1, 22.9,

14.5. IR (ATR): ν, cm-1 2232 (–CN).

8. Compound **8** was synthesized from 4,5-dichlorophthalonitrile and 2-ethynyl-3-hexylthiophene by the same procedure as for **5**. Yield 25%. ^{1}H NMR ($CDCl_3$, 400.13 MHz): δ, ppm 7.89 (1H, s, ArH), 7.85 (1H, s, ArH), 7.37 (1H, d, *J* = 5.2 Hz, ArH), 6.96 (1H, d, *J* = 5.2 Hz, ArH), 2.81 (2H, t, *J* = 7.6 Hz, –CH_2–), 1.63–1.70 (2H, m, –CH_2–), 1.28–1.37 (6H, m, –CH_2–), 0.88 (3H, t, *J* = 6.8 Hz, –CH_3). ^{13}C NMR ($CDCl_3$, 100.61 MHz): δ, ppm 152.1, 140.4, 136.7, 134.4, 130.0, 129.8, 129.2, 116.4, 114.7, 114.6, 96.4, 90.3, 32.0, 30.7, 30.3, 29.4, 23.0, 14.5. IR (ATR): ν, cm^{-1} 2232 (–CN).

Phthalocyanines

Cu-9. A mixture of **5** (150 mg, 0.55 mmol), urea (67 mg, 1.1 mmol), and $Cu(OAc)_2$ H_2O (28 mg, 0.14 mmol) in *N*,*N*′-dimethylpropyleneurea (3.0 mL) was heated at 160 ºC for 12 h under N_2 atmosphere. After cooling to 60 ºC, methanol was added to the reaction mixture and stirred for 15 min. The resulting suspension was filtered off and washed with methanol. The solid residue was purified by column chromatography on activated alumina by eluting with $CHCl_3$ and recycling preparative HPLC to give Cu-**9** (53 mg, 33%). UV-vis (10 mM in $CHCl_3$): λ, nm 628 and 695. MALDI-TOF MS (dithranol): *m/z* 1146.5 ([M + H], 100%), calcd. for $C_{64}H_{60}Cl_4N_8Cu$: *m/z* 1146.6.

Zn-9. Zn-**9** was synthesized from **5** and $Zn(OAc)_2$ by the same procedure as for Cu-**9**. Yield 55%. UV-vis (10 mM in $CHCl_3$): λ, nm 696. ^{1}H NMR ($CDCl_3$, 400.13 MHz): δ, ppm 8.5–9.0 (4H, br, ArH), 6.4–6.7 (4H, br, ArH), 2.7– 2.9 (8H, m, –CH_2–), 1.7–2.0 (16H, m, –CH_2–), 1.0–1.2 (16H, m, –CH_2–), 0.8 (12H, br, –CH_3). MALDI-TOF MS (dithranol): *m/z* 1148.4 ([M + H], 100%), calcd. for $C_{64}H_{60}Cl_4N_8Zn$: *m/z* 1148.4.

Cu-10. Cu-**10** was synthesized from **6** and $Cu(OAc)_2$ H_2O by the same procedure as for Cu-**9**. Yield 49%. UV-vis (10 mM in $CHCl_3$): λ, nm 634 and 710^{sh}. MALDI-TOF MS (dithranol): *m/z* 1449.2 ([M + H], 100%), calcd. for $C_{88}H_{76}Cl_4N_8Cu$: *m/z*

1450.9.

Zn-10. Zn-**10** was synthesized from **6** and $Zn(OAc)_2$ by the same procedure as for Cu-**9.** Yield 51%. UV-vis (10 mM in $CHCl_3$): λ, nm 655 and 705. ^1H NMR ($CDCl_3$, 400.13 MHz): δ, ppm 6.4–9.0 (24H, br, ArH), 3.5–3.9 (8H, m, $–CH_2–$), 2.3– 2.6 (8H, m, $–CH_2–$), 1.6–1.9 (8H, m, $–CH_2–$), 1.2–1.4 (16H, m, $–CH_2–$), 0.8 (12H, br, $–CH_3$). MALDI-TOF MS (dithranol): *m/z* 1452.2 ([M + H], 100%), calcd. for $C_{88}H_{76}Cl_4N_8Zn$: *m/z* 1452.8.

Cu-11. Cu-**11** was synthesized from **7** and $Cu(OAc)_2$ H_2O by the same procedure as for Cu-**9**. Yield 49%. UV-vis (10 mM in $CHCl_3$): λ, nm 644 and 712^{sh}. MALDI-TOF MS (dithranol): *m/z* 1472.7 ([M + H], 100%), calcd. for $C_{80}H_{68}Cl_4N_8S_4Cu$: *m/z* 1471.2.

Cu-12. Cu-**12** was synthesized from **8** and $Cu(OAc)_2$ H_2O by the same procedure as for Cu-**9**. Yield 66%. UV-vis (10 mM in $CHCl_3$): λ, nm 648 and 711. MALDI-TOF MS (dithranol): *m/z* 1473.7 ([M + H], 100%), calcd. for $C_{80}H_{68}Cl_4N_8S_4Cu$: *m/z* 1471.2.

Thiophene-fused phthalocyanines

Cu-1. A mixture of Cu-**9** (27 mg, 0.23 mmol), NaS $9H_2O$ (45 mg, 18.8 mmol) in *N*-methylpyrrolidone (5.0 mL) was stirred at 190 ºC with stirring for 12 h under N_2 atmosphere. After cooling to room temperature, the reaction mixture was poured into 50 mL saturated NH_4Cl aqueous solution and stirred for 30 min. The resulting suspension was filtered off and washed with methanol. The solid residue was purified by column chromatography on activated alumina by eluting with $CHCl_3$ and recycling preparative HPLC to give Cu-**1** (11 mg, 41%). UV-vis (10 mM in $CHCl_3$): λ, nm 669 and 726. MALDI-TOF MS (dithranol): *m/z* 1135.1 ([M + H], 100%), calcd. for $C_{64}H_{64}N_8S_4Cu$: *m/z* 1135.4. Elemental analysis calcd. (%) for $C_{64}H_{64}N_8S_4Cu$: C 67.60, H 5.67, N 9.85; found C 67.7, H 5.7, N 9.7. Purity (HPLC) > 99%.

Zn-**1**, Cu-**2**, Zn-**2**, Cu-**3**, and Cu-**4** were synthesized by the same procedure as for

Cu-**1**.

Zn-1. Yield 24%. UV-vis (10 mM in $CHCl_3$): λ, nm 670sh and 734. ^1H NMR ($CDCl_3$, 400.13 MHz): δ, ppm 6.6–8.5 (12H, br, ArH), 3.6–3.8 (16H, m, $–CH_2–$), 2.0 (8H, br, $–CH_2–$), 1.3 (16H, br, $–CH_2–$), 0.7 (12H, br, $–CH_3$). MALDI-TOF MS (dithranol): *m/z* 1137.3 ([M + H], 100%), calcd. for $C_{64}H_{64}N_8S_4Zn$: *m/z* 1136.3. Elemental analysis calcd. (%) for $C_{64}H_{64}N_8S_4Zn$: C 67.50, H 5.66, N 9.84; found C 67.6, H 5.6, N 9.7. Purity (HPLC) > 99%.

Cu-2. Yield 36%. UV-vis (10 mM in $CHCl_3$): λ, nm 665 and 740^{sh}. MALDI-TOF MS (dithranol): *m/z* 1441.4 ([M + H], 100%), calcd. for $C_{88}H_{80}N_8S_4Cu$: *m/z* 1441.4. Elemental analysis calcd. (%) for $C_{88}H_{80}N_8S_4Cu$: C 73.33,

H 5.59, N 7.77; found C 73.4, H 5.6, N 7.8. Purity (HPLC) > 99%.

Zn-2. Yield 25%. UV-vis (10 mM in $CHCl_3$): λ, nm 682 and 735. ^1H NMR ($CDCl_3$, 400.13 MHz): δ, ppm 6.6–8.5 (28H, br, ArH), 3.6–3.8 (8H, m, $–CH_2–$), 2.4–2.6 (8H, m, $–CH_2–$), 1.9 (8H, br, $–CH_2–$), 1.3 (16H, br, $–CH_2–$), 0.9 (12H, br, $–CH_3$). MALDI-TOF MS (dithranol): *m/z* 1443.4 ([M + H], 100%), calcd. for $C_{88}H_{80}N_8S_4Zn$: *m/z* 1443.3. Elemental analysis calcd. (%) for $C_{88}H_{80}N_8S_4Zn$: C 73.23, H 5.59, N 7.76; found C 73.3, H 5.6, N 7.7. Purity (HPLC) > 99%.

Cu-3. Yield 50%. UV-vis (10 mM in $CHCl_3$): λ, nm 670^{sh} and 734. MALDI-TOF MS (dithranol): *m/z* 1463.3 ([M + H], 100%), calcd. for $C_{80}H_{72}N_8S_8Cu$: *m/z* 1463.3. Elemental analysis calcd. (%) for $C_{80}H_{72}N_8S_8Cu$: C 65.57, H 4.95, N 7.65; found C 65.5, H 5.0, N 7.6. Purity (HPLC) > 99%.

Cu-4. Yield 43%. UV-vis (10 mM in $CHCl_3$): λ, nm 682 and 735. MALDI-TOF MS (dithranol): *m/z* 1464.7 ([M + H], 100%), calcd. for $C_{80}H_{72}N_8S_8Cu$: *m/z* 1463.3. Elemental analysis calcd. (%) for $C_{80}H_{72}N_8S_8Cu$: C 65.57, H 4.95, N 7.65; found C 65.6, H 4.9, N 7.7. Purity (HPLC) > 99%.

2.3 Results and Discussion

2.3.1 Syntheses of thiophen-fused metallophthalocyanines

Scheme 1*. Syntheses of Thiophene-fused MPcs* ***1-4****.*

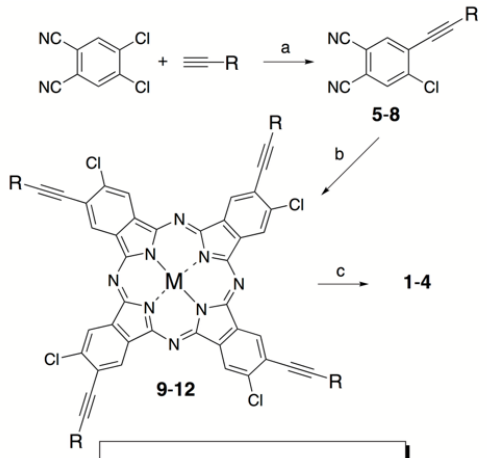

(a) $PdCl_2(PPh_3)_2$, CuI, triethylamine-THF, (b) $M(AcO)_2$, urea, *N,N'*-dimethyl-propyleneurea, (c) Na_2S $9H_2O$, NMP. MPcs **1-4** and **9-12** contain structural isomers.

Scheme 1 illustrates the synthetic route of thiophene-fused MPcs **1–4**. Phthlocyanine precursors **5–8** were synthesized through palladium-catalyzed Sonogashira coupling of 4,5-dichlorophthalonitrile with alkynes. MPcs **9–12** fused with *o*-chloroethynylbenzene were prepared in the presence of metal salts, and the final ring closing reaction with sodium sulfide[22] obtained **1–4** in good yields. The MALDI-TOF-Ms spectra of all final compounds exhibited the expected parent molecular ion peak, and their purities were confirmed by HPLC analyses. All MPcs decorated with four flexible substituents at the α-positions of the fused thiophene rings revealed good solubility (>10 g L^{-1}) in organic solvents such as THF, toluene and $CHCl_3$.

2.3.2 Optical and electrochemical properties

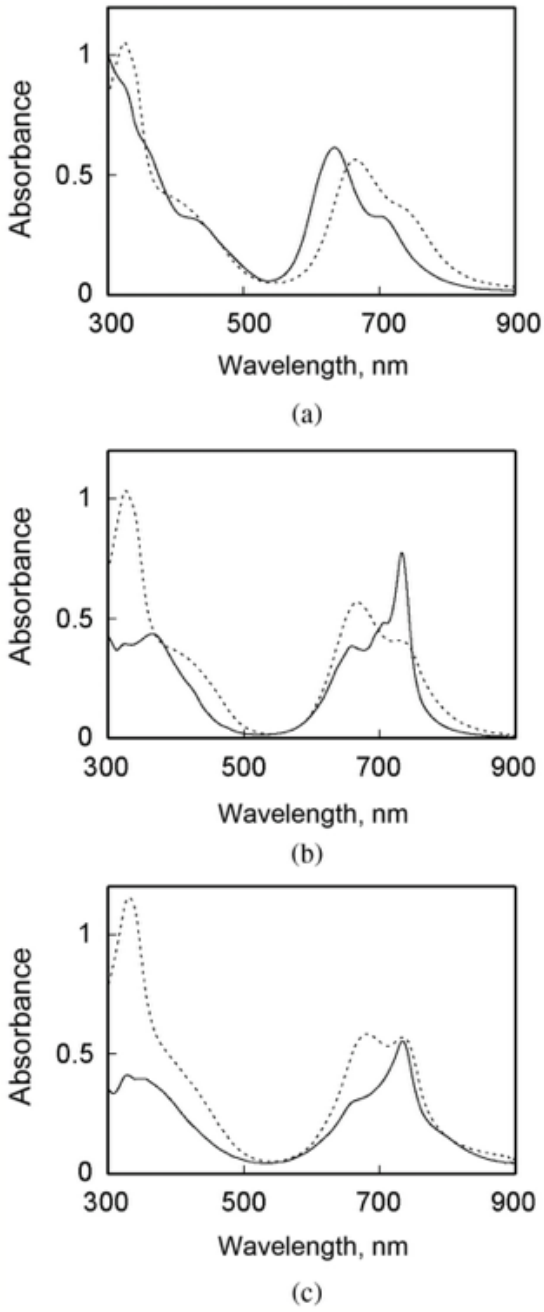

Fig. 2. *Absorption spectra of a) Cu-**10** (solid line) and Cu-**2** (dashed line) in $CHCl_3$, b) Cu-**1** (solid line) and Cu-**2** (dashed line) in 1,3,5-trimethylbenzene, and c) Zn-**1** (solid line) and Zn-**2** (dashed line) in $CHCl_3$. [MPcs] = 10 μM.*

The shape and location of the Q-band of MPcs are known to be indicators for determining the aggregation behavior of MPcs. All CuPcs exhibit a broad absorption Q-band in the range of 550–850 nm in $CHCl_3$ (Fig. 2a and Table 1). The broadening of the Q-band is caused by exciton coupling between neighboring phthalocyanine rings in aggregates.[23] No changes on the absorption spectral shape in $CHCl_3$ were detected in the concentration range of 5 μM to 0.1 mM, indicating the formation of stable aggregates in solution. The absorption maxima of the Q-bands for thiophene-fused CuPcs **1**–**4** shift to longer wavelengths relative to the parent compounds. The red-shifting of Q-band is ascribed to the enlargement of the π-conjugated system by fusing thiophenes with the phthalocyanine ring. The Q-bands of Cu-**3** and Cu-**4** were red-shifted as compared with the spectra of Cu-**1** and Cu-**2** due to the attachment of electron-donating thiophene spacers with thiophene-fused phthalocyanine ring (Fig. 3).

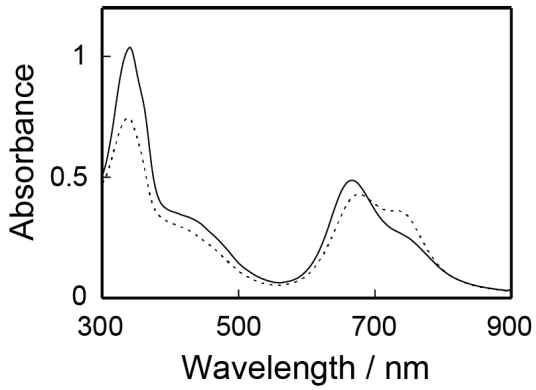

***Fig. 3**. Absorption spectra of Cu-**3** (solid line) and Cu-**4** (dashed line) in $CHCl_3$. [MPcs] = 10 μM.*

Fig. 2b shows the absorption spectra of Cu-**1** and Cu-**2** in 1,3,5-trimethylbenzene. The spectrum of Cu-**1** in 1,3,5-trimethylbenzene displayed a peak at 733 nm, indicating the dissociation of aggregates into monomeric species caused by solvent changing. In contrast, the Q-bands of Cu-**2** remained unaltered in

1,3,5-trimethylbenzene. The aggregation properties in solution were enhanced by the presence of phenyl spacer in the solubilizing side chains. Whereas Cu-**1** exhibits a broad Q-band in $CHCl_3$, the peak at 734 nm is observed in the spectrum of Zn-**1** (Fig. 2c). The difference in the aggregation behavior reflected the attracting force between MPcs that had different central metals. The attracting force between CuPcs was stronger than that between ZnPcs.

Table 1. *Photophysical and electrochemical data for MPcs* ***1-4***.

Ligand	Metal	λ_{max}, nm[a]	$E_{1/2}$, V *vs. Fc/Fc*$^{+}$[b]
1	Cu	669, 726[sh]	0.14, 0.83
	Zn	670[sh], 734	0.14, 1.03
2	Cu	665, 740[sh]	0.12, 0.90
	Zn	682, 735	0.13, 1.14
3	Cu	672, 750[sh]	0.14, 1.02
4	Cu	677, 750[sh]	0.14, 1.02

[a] In $CHCl_3$. [b] Determined by differential pulse voltammetry in CH_2Cl_2 containing 0.1 M Bu_4NClO_4 at 295 K, scan rate = 50 mV/s [sh] Shoulder peak.

Electrochemical studies of thiophene-fused MPcs were performed through cyclic voltammetry measurement in CH_2Cl_2 containing 0.1M Bu_4NClO_4 as a supporting electrolyte (Table 1). Cu-**1** exhibits two reversible oxidation waves at +0.14 and +0.83 V *vs.* ferrocene/ ferrocenium redox couple (*Fc/Fc*$^{+}$). Since Cu(II) does not undergo a redox process within the potential window in CH_2Cl_2, the observed oxidation processes can be ascribed to thiophene-fused phthalocyanine-centered ring oxidations.[24] The highest occupied molecular orbital (HOMO) energy levels of Cu-**1** and Cu-**2** were estimated to be -4.94 and -4.92 eV from the first oxidation potentials calibrated by the *Fc/Fc*$^{+}$ redox potential *vs.* vacuum (Table 1). The HOMO energy levels of Cu-**1** and Cu-**2** were slightly higher than that of copper phthalocyanines (HOMO = -5.2 eV). The enlargement of π-system resulted in the destabilization of the HOMO.

2.3.3 Self-assembly properties

Phthalocyanines substituted with linear or branched alkyl, alkoxymethyl, or alkoxy chains form a major class of discotic liquid-crystalline materials that self-organize in columnar stacks.[25-29] The type of side chain, its length, the symmetry of Pc molecule influence the self-organized structure. The self-organizing properties of Cu-**1** and Cu-**2** were investigated by differential scanning calorimetry (DSC), temperature-controlled polarized optical microscopy (TPOM), and X-ray diffraction (XRD). No typical textures in TPOM and no transitions in DSC were observed in Cu-**1** and Cu-**2** on heating and cooling from -50 to 250 ºC. The number and length of alkyl chains in Cu-**1** and Cu-**2** are not sufficient to exhibit liquid crystal phases.

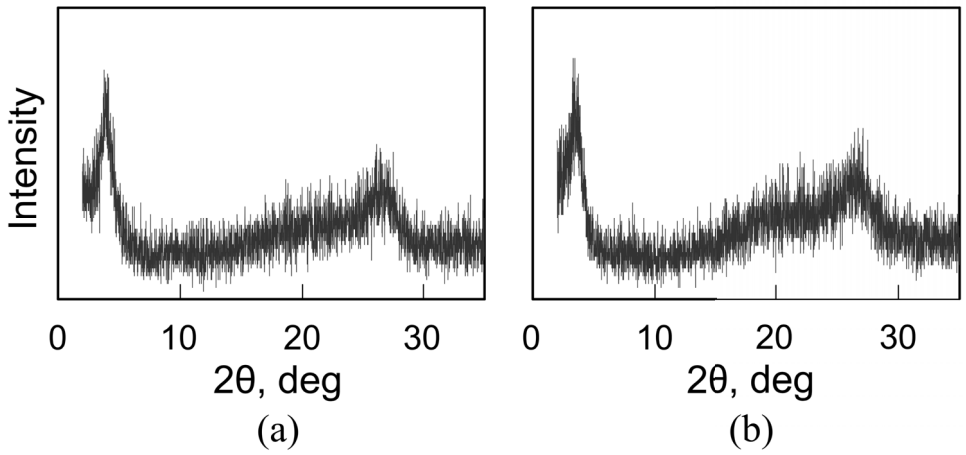

Fig. 4. *XRD patterns of a) Cu-**1** and b) Cu-**2** at room temperature*.

As shown in Fig. 4, the XRD patterns of Cu-**1** and Cu-**2** at room temperature show one reflection peak corresponding to the *d* spacing of 2.23 and 2.53 nm, which is attributed to the average distance between stacked columns in the solid. Cu-**2** with phenyl spacer has a longer average distance than Cu-**1**. Since the XRD patterns in the small angle region showed only one peak, two- or three-dimensional

lattices could not be assigned from the XRD patterns. The reflection peak at 0.33 nm characteristic of the π–π stacking is observed, thus indicating a long-range ordering along the columnar axis. The broad and diffuse halo around 0.43 nm can be ascribed to the liquid-like disorder in alkyl chains.

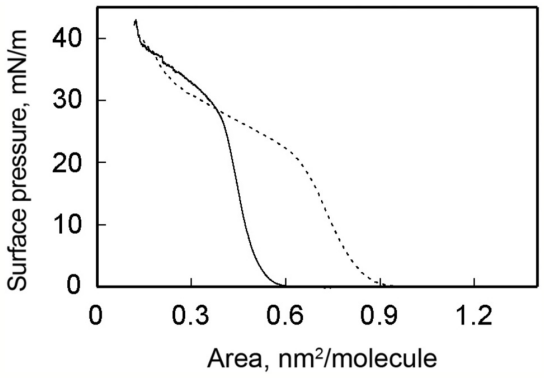

Fig. 5. *Surface pressure vs. area per molecule isotherms for Cu-**1** (solid line) and Cu-**2** (dashed line) on triply distilled water at 25 °C.*

The organized structures of Cu-**1** and Cu-**2** were analyzed by a surface pressure *vs*. area (π-A) isotherm on pure water as the substrate (Fig. 5).[30] A continuous rise in the pressure as the area decreased was observed up to 40 mN m^{-1}, whereupon the monomolecular film collapsed. The limiting surface areas per molecules of Cu-**1** and Cu-**2** were 0.52 and 0.84 nm^2/molecule determined by extrapolating the slope of the π-A isotherms in the liquid- condensed region to zero pressure. The limiting surface area of Cu-**2** mostly agreed with the area occupied in an edge-on arrangement of molecules on the water surface. This indicates that Cu-**2** forms stacks with phthalocyanine plane perpendicular to the air-water interface. In contrast, the limiting area of Cu-**1** is smaller than the estimated edge area (0.74 nm^2), suggesting the formation of slipped stacks on the interface.[31]

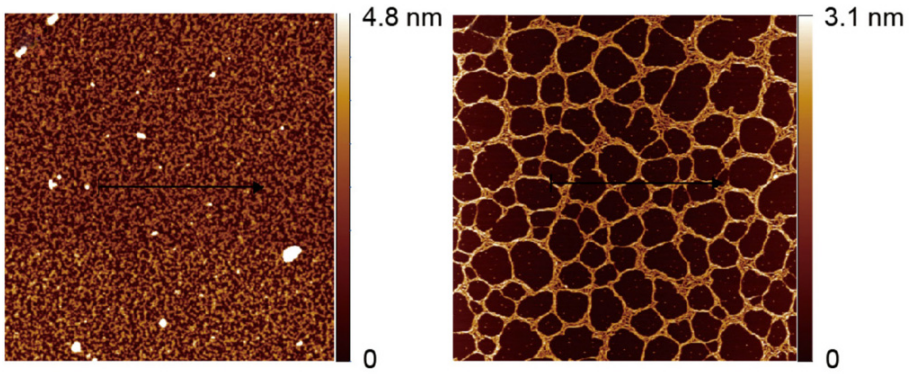

(a) (b)

Fig. 6. *AFM images (area: 5 × 5 μm) of a) Cu-**1** and b) Cu-**2** on mica substrates*.

The organized morphologies of Cu-**1** and Cu-**2** were visualized by atomic force scanning microscopy (AFM) (Fig. 6). A droplet of 5×10^{-5} M solutions of Cu-**1** or Cu-**2** in $CHCl_3$ was placed on a mica substrate, and the solution was evaporated in vacuum. Although the AFM height image of Cu-**1** shows no featured dots, Cu-**2** assembled into network structures of fibers with a 2.4 nm height. The fibers consist of bundles of finer strands, and some isolated single strands can be seen. The length of fibers is in an order of a few micrometers. The observed height of fibers is in fair agreement with the average intercolumnar distance as obtained from the XRD analysis and the diameter of molecular model of Cu-**2**. These results may conclude that Cu-**2** self-assembles in $CHCl_3$ solution to produce long one-dimensional stacks. The phenyl spacers in Cu-**2** enhance the attracting force among molecules, and the enhanced attracting force induces the formation of nanoscopic fibers in solution. On the other hand, Cu-**1** assembles short stacks in solution relative to Cu-**2**. The short stacks result in the slipped stacks in air-water interface and the dotted structures on mica.

2.3.4 OFET properties

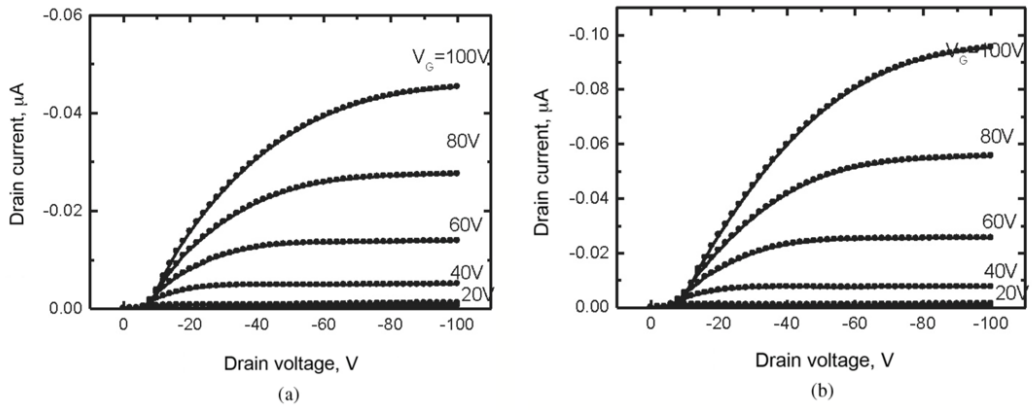

Fig. 7. *Drain-source current vs. drain-source voltage characteristics for a) Cu-**1** and b) Cu-**2**.*

Solution-processed OFETs using Cu-**1** and Cu-**2** were fabricated using the top-contact device configuration. Thin films were deposited onto a Si/SiO_2 substrate with hydrophobic surface treatment using an insulating polymer by spin coating using 20 mg/mL solutions of Cu-**1** or Cu-**2** in $CHCl_3$ containing 1.0 wt% 1,3,5-trichlorobenzene at 1000 rpm for 40 sec. In AFM images, the obtained thin films appeared to be smooth and have a homogeneous surface with a surface roughness RMS of less than 0.3 nm in the region of 3 × 3 mm. Gold source and drain electrodes with 70 nm thickness were vapor-deposited on top of the thin films. The channel length and the width of the source and drain electrodes were 50 mm and 5.5 mm, respectively. FET characteristics were measured in a nitrogen glove box system. Both the Cu-**1** and Cu-**2** devices showed typical p-channel FET responses (Fig. 7). The field-effect mobilities measured in the saturation regime were 1.06×10^{-5} cm^2 V^{-1} s^{-1} for Cu-**1** and 2.37×10^{-5} cm^2 V^{-1} s^{-1} for Cu-**2** with I_{on}/I_{off} of 10^2–10^3. The device performance is lower than the reported values for phthalocyanine-based OFETs.[19, 32-38] The XRD patterns of spin-coated films on the Si/SiO_2 substrate revealed broad reflection peaks, indicating their low crystallinity. The low crystallinity of thin films results in low performance of OFETs.

2.3.5 Electrochemical polymerization

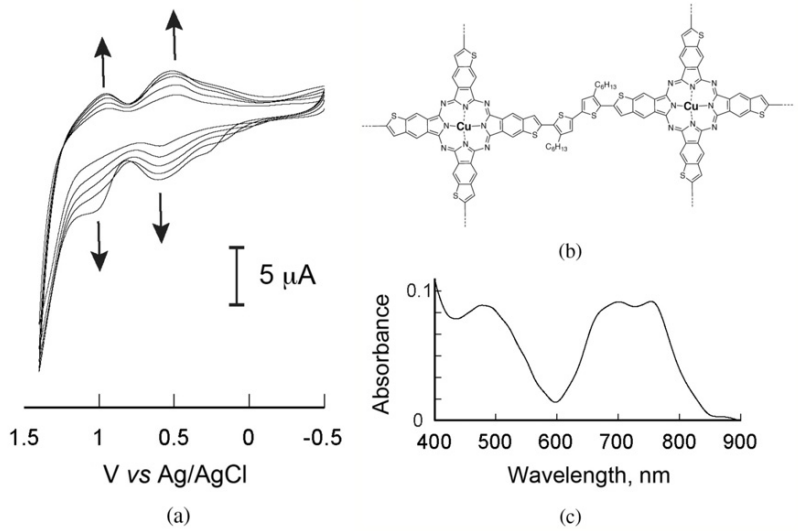

Fig. 8. *a) Repeated CV cycles of Cu-**4** in CH_2Cl_2 containing 0.1 M Bu_4NPF_6 (scan rate: 100 mV s^{-1}). b) Network structure of electropolymerized Cu-**4**. c) Absorption spectrum of electropolymeized Cu-**4** deposited onto an ITO electrode.*

The terminal α-positions in Cu-**4** are available for electrochemical polymerization to produce cross-linked films. Electrochemical polymerization provides a convenient way for redox-active monomers to deposit a polymer film directly onto the surface of electrodes.[39-41] The electrochemical polymerization of Cu-**4** was performed in a three-electrode cell using platinum as a counter electrode, Ag/AgCl as a reference electrode, and ITO-coated glass substrate as a working electrode. Cu-**4** was electrodeposited as film using 0.1 M concentration of CH_2Cl_2 containing 0.1 M Bu_4NPF_6 as a supporting electrolyte and scanning between -0.5 and 1.4 V at a scan rate of 50 mV/s. The polymer film of Cu-**4** on an ITO electrode was prepared by five cycles of potential scans. Two reversible oxidation waves at 0.53 and 1.04 V *vs.* Ag/AgCl were observed (Fig. 8a). The peak currents increased upon the repeated scans and a yellow-green film was deposited onto the surface of an ITO electrode. The resulting film on ITO is designated as polymerized Cu-**4**. Since

four thiophene terminals in Cu-**4** could undergo the oxidative coupling reaction, the resulting polymers possess a three-dimensional network, where the thiophene-fused CuPcs are connected with bithiophene segments in the network polymer. The polymerized films were rinsed with CH_2Cl_2 to remove any residual soluble species (Fig. 8b). The rinsed films exhibited two oxidation waves at the same positions as observed in the electrochemical polymerization of Cu-**4**, and less than 5% loss of electroactivity after 50 repeated scans between 0 and 1.4 V in monomer-free electrolyte solution. The absorption spectrum of polymerized Cu-**4** is almost the same as that of Cu-**4** in solution, suggesting the stacking of CuPcs within the three-dimensional network (Fig. 8c).[42-44]

2.4 Conclusion

In summary, the author has synthesized thiophene-fused phthalocyanines **1**–**4** through the ring closing reaction from the *o*-chloroethynylbenzene substructures. The self-organizing properties of thiophene-fused phthalocyanines were investigated in solution, at air-water interface, and in the solid state. The attachment of *n*-hexylphenyl units at α-positions of the fused thiophene rings creates the network structure of nanoscopic fibrous assemblies with excellent long-range stacking through the intermacrocycle interaction with the additional interaction between peripheral phenyl spacers. Cu-**1** and Cu-**2** acted as a soluble p-channel organic semiconductor, but the field-effect mobility was not high due to the low crystallinity in the solid state. Cu-**4** possessing thiophene spacers was polymerized into the electrochemically active films onto an electrode by the connection of four thiophene terminals through the oxidative coupling reaction. Further structural modifications of thiophene-fused phthalocyanines to control molecular ordering in the solid phase are now underway in our group.

2.5 References

1. Arias AC, MacKenzie JD, McCulloch I, Rivnay J and Salleo A. *Chem. Rev.* 2010; **110**: 3.
2. Habas S, Platt HAS, van Hest FAM and Ginley DS. *Chem. Rev.* 2010; **110**: 6571.
3. WenY, LiuY, GuoY,Yu G and Hu W. *Chem. Rev.* 2011; **111**: 3358.
4. Mas-Torrent M and Rovira C. *Chem. Rev.* 2011; **111**: 4833.
5. Minemawari H, Yamada T, Matsui H, Tsutsumi J, Haas S, Chiba R, Kumai R and Hasegawa T. *Nature* 2011; **475**: 364.
6. Babu SS, Prasanthkumar S and Ajayaghosh A. *Angew. Chem. Int. Ed.* 2011; **51**: 1766.
7. Takimiya K, Shinamura S, Osaka I and Miyazaki E. *Adv. Mater.* 2011; **23**: 4347 and related references therein.
8. Takimiya K, Kunugi Y, Konda Y, Niihara N and Otsubo T. *J. Am. Chem. Soc.* 2004; **126**: 5084.
9. Ebata H, Izawa T, Miyazaki E, Takimiaya K, Ikeda M, Kuwabara H and Yui T. *J. Am. Chem. Soc*., 2007; **129**: 15732.
10. Izawa T, Miyazaki E and Takimiya K. Adv. Mater. 2008; **20**: 3388.
11. Shinamura S, Osaka I, Miyazaki E, Nakao A, Yamagishi M, Takeya J and Takimiya K. *J. Am. Chem. Soc.* 2011; **133**: 5024.
12. Kaafarani BR. *Chem. Mater.* 2011; **23**: 378.
13. van Nostrum CF, Picken SJ, Schouten AJ and Nolte RJM. *J. Am. Chem. Soc.* 1995; **117**: 9957.
14. Smolenyak P, Peterson R, Nebesny K, Törker M, O'Brien DF and Armstrong NR. *J. Am. Chem. Soc.* 1999; **121**: 8628.
15. Kimura M, Muto T, Takimoto H, Wada K, Ohta K, Hanabusa K, Shirai H and Kobayashi N. *Langmuir* 2000; **16**: 2078.
16. Kimura M, Wada K, Ohta K, Hanabusa K and Shirai H. *J. Am. Chem. Soc.* 2001; **123**: 2438.
17. de la Escosura A, Martínez-Díaz MV, Thordarson P, Rowan AE, Nolte RJM and Torres T. *J. Am. Chem. Soc.* 2003; **125**: 12300.

18. Cook MJ and Jafari-Fini A. *J. Mater. Chem.* 1997; **7**: 5.
19. Miyazaki E, Kaku A, Mori H, Iwatani M and Takimiya K. *J. Mater. Chem.* 2009; **19**: 5913.
20. Taraimovich ES, Stuzhin PA and Koifman OI. *Russ. J. Gen. Chem.* 2013; **83**: 392.
21. Dubinina TV, Dyumaeva DV, Trashin SA, Sedova MV, Dudnik AS, Borisova NE, Tomilova LG and Zefirov N. *Dyes Pigm.* 2013; **96**: 699.
22. Kashiki T, Shinamura S, Kohara M, Miyazaki E, Takimiya K, Ikeda M and Kuwabara H. *Org. Lett.* 2009; **11**: 2473.
23. Stillman MJ and Nyokong T. *Phthalocyanines Properties and Applications*, Vol. 1, Leznoff CC and Lever ABP. (Eds.) VCH: New York, 1989; pp 135.
24. Lever ABP, Milaeva ER and Speier G. *Phthalocyanines Properties and Applications*, Vol. 3, Leznoff CC and Lever ABP. (Eds.) VCH: New York, 1993; pp 3.
25. Piechocki C, Simon J, Skoulios A, Guillon D and Weber P. *J. Am. Chem. Soc*. 1982; **104**: 5245.
26. Clarkson GJ, Cook A, McKeown NB, Treacher K and Ali-Adib Z. *Macromolecules* 1996; 29: 913.
27. Ohta K, Yamaguchi N and Yamamoto I. *J. Mater. Chem.* 1998; **8**: 2637.
28. Kimura M, Kuroda T, Ohta K, Hanabusa K, Shirai H and Kobayashi N. *Langmuir* 2003; **19**: 4825.
29. De Cupere V, Tant J, Viville P, Lazzaroni R, Osikowicz W, Salaneck WR and Geerts YH. *Langmuir* 2006; **22**: 7798.
30. Cook MJ and Chambrier I. *The Porphyrin Handbook*, Vol. 17, Kadish KM, Smith KM and Guilard R. (Eds.) Academic Press: San Diego, CA, 2000; pp 37.
31. Kobayashi N, Lam H, Nevin WA, Janda P, Leznoff CC, Koyama T, Monden A and Shirai H. *J. Am. Chem. Soc.* 1994; **116**: 879.
32. Bao Z, Lovinger AJ and Dodabalapur A. *Appl. Phys. Lett.* 1996; **69**: 3066.
33. Bao Z, Lovinger AJ and Brown J. *J. Am. Chem. Soc.* 1998; **120**: 207.
34. Xiao K, LiuY, Huang X, XuY,Yu G and Zhu D. *J. Phys. Chem. B* 2003; **107**: 9226.

35. Zhang J, Wang J, Wang H and Yan D. *Appl. Phys. Lett.* 2004; **84**: 142.
36. Su W, Jiang J, Xiao K, ChenY, Zhao Q,Yu G and Liu Y. *Langmuir* 2005; **21**: 6527.
37. Tang ML, Oh JH, Reichardt AD and Bao Z. *J. Am. Chem. Soc.* 2009; **131**: 3733.
38. Kim Sh, Ko HC, Moon B and Lee H. *Langmuir* 2006; **22**: 9431.
39. Ponnapati R, Felipe MJ and Advincula R. *Macromolecules* 2011; **44**: 7530.
40. Kimura M, Sakai R, Sato S, Fukawa T, Ikehara T, Maeda R and Mihara T. *Adv. Funct. Mater.* 2012; **22**: 469.
41. Liu TA, Prabhakar C, Yu JY, Chen Ch, Huang HH and Yang JS. *Macromolecules* 2012; **45**: 4529.
42. Kimura M, Horai T, Hanabusa K and Shirai H. *Chem. Lett.* 1997; **26**: 653.
43. Obirai J, Rodrigues NP, Bedioui F and Nyokong T. *J. Porphyrins Phthalocyanines* 2003; **7**: 508.
44. Kimura M, Yasuta K, Adachi N, Tatewaki Y, Fukawa T and Shirai H. *Chem. Lett.* 2009; **38**: 82.

Chapter 3

Topological control of columnar stacking made of liquid-crystalline thiophene-fused metallonaphthalocyanines

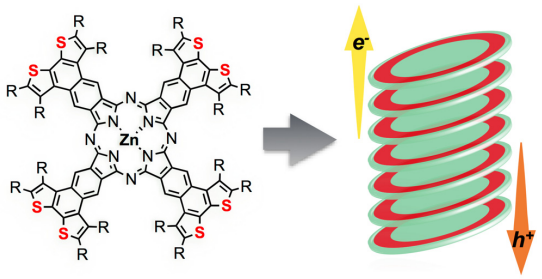

Abstract

Two structural regioisomers of thiophene-fused zinc naphthalocyanines **ZnTNc$_{endo}$** and **ZnTNc$_{exo}$** have been designed and synthesized to obtain photo- and electroactive liquid crystalline materials. Both compounds exhibited liquid crystalline behavior over a wide temperature range through intermolecular π-π interactions and local phase segregation between the aromatic cores and peripheral side chains. The structural differences between **ZnTNc$_{endo}$** and **ZnTNc$_{exo}$** affected the stacking mode in self-assembled columns as well as symmetry of the two-dimensional rectangular columnar lattice. The columnar structure in liquid crystalline phase exhibited an ambipolar charge-transport behavior. The enlargement of the π-conjugated core and the control of self-organized nanostructures enhanced the carrier mobilities.

3.1 Introduction

Spontaneous organization of two-dimensional polyaromatic molecules into well-defined nanostructures through non-covalent interactions has been intensively explored, to realize organic-based electronic and optoelectronic devices.[1-3] The decoration of polyaromatic cores with flexible alkyl chains results in the formation of liquid-crystalline phases, which correspond to one-dimensional columnar stacks of polyaromatic molecules driven by the intermolecular π-π interactions and the local phase segregation between the flat rigid aromatic cores and peripheral side chains.[4,5] The intermolecular π-π overlap among polyaromatic molecules within the columns provides a transport pathway for charge or energy along the columnar axis. The charge carrier mobilities and semiconductivities can be tailored by designing polyaromatic cores and controlling the self-organization of molecules in the bulk.

Metallophthalocyanines (MPcs) and their analogues have been widely used as a molecular material in applications from organic pigments to semiconductors for electronic devices because of their unique optical properties and thermal stability.[6,7] Since the first report of liquid crystalline Pc by Piechocki and Simon[8], liquid crystalline MPcs have been modified to control the self-organized nanostructures, and applied as molecular components in organic thin-film transistors (OTFT) and solar photovoltaics (OPV).[9,10] The optical and electronic properties of MPcs strongly depend on the size of the π-system.[11] The expansion of the phthalocyanine π-system has been achieved by condensation of fused polyaromatic precursors.[12-18] The size and geometry of the annulated aromatic residues on the tetraazaporphyrin core affect the position of the Q band, as well as the HOMO and LUMO energy levels. Moreover, the expansion of the π-system enhances the tendency for π-stacking. Although various ring-expanded MPcs with alkyl chains have been synthesized and their self-assembly properties in solution or on substrates investigated, there have been few reports on the spontaneous organization of liquid

crystalline ring-expanded MPcs into nanostructures. [19-22]

In this chapter, the author reports the syntheses of two isomeric, thiophene-fused zincnaphthalocyanines (Nc), **ZnTNc$_{endo}$** and **ZnTNc$_{exo}$** decorated with sixteen dodecyl chains, and their self-organization properties. Thiophene-fused polyaromatic molecules display excellent performance in OTFT and OPV, due to the formation of three-dimensional molecular stacks through sulfur-sulfur contact between thiophene segments.[23,24] The author hoped to control the organized structure of ring-expanded MPcs and enhance the charge mobilities by fusing with thiophene rings at the peripheral positions of the Nc ring. The physical properties and self-organized structures in the liquid crystalline phase, and the carrier mobilities of the two isomers were compared with each other.

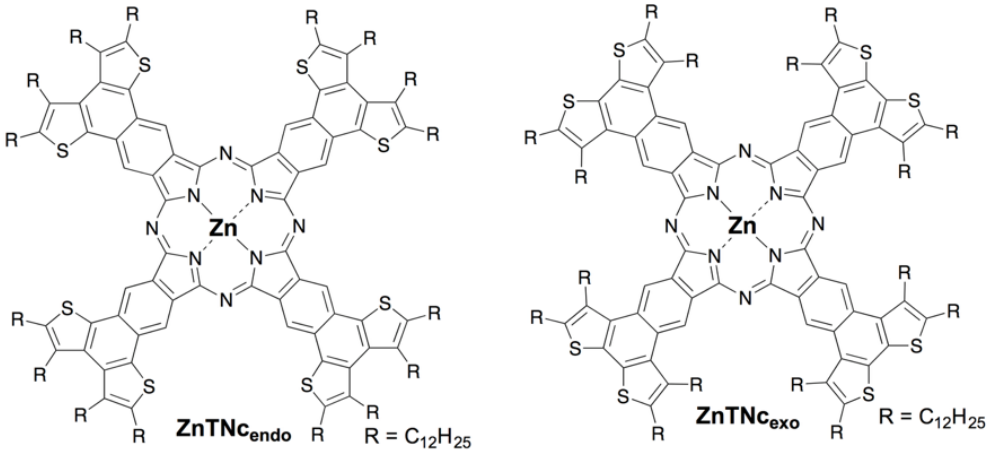

Chart. ***ZnTNc$_{endo}$*** *and* ***ZnTNc$_{exo}$.***

3.2 Experimental section

3.2.1 General procedures

NMR spectra were recorded on a Bruker AVANCE 400 FT NMR spectrometer at 399.65 MHz and 100.62 MHz for ^{1}H and ^{13}C in $CDCl_3$ solution. Chemical shifts are reported relative to internal TMS. IR spectra were obtained on a SHIMAZU IR Prestige-21 with DuraSample IR II. Absorption spectra were measured on a SHIMAZU UV-2600. MALDI-TOF mass spectra were obtained on a Bruker Autoflex spectrometer with dithranol as matrix.

All chemicals were purchased from commercial suppliers and used without further purification. 2-Bromo-4,5-didodecylthiophene was synthesized according to the literature method.[26] Column chromatography was performed with activated alumina (Wako, 200mesh) or silica gel (Wakogel C-200). Recycling preparative gel permeation chromatography was carried out by a JAI recycling preparative HPLC using $CHCl_3$ as an eluent. Analytical thin layer chromatography was performed with commercial Merck plates coated with silica gel 60 F_{254} or aluminum oxide 60 F_{254}.

3.2.2 Syntheses

Replacement of substitution position[26,27]

3-Bromo-4, 5-didodecylthiophene **1**: To a solution of diisopropylamine (1.43 mL, 10.2 mmol) in THF (60 mL) was slowly added *n*-butyllithium (1.6 M in hexanes, 4.5 mL, 7.20 mmol), and the reaction kept for 30 min at 0 ºC under an Ar atmosphere. A solution of 2-bromo-4,5-didodecylthiophene (3.0 g, 6.00 mmol) in THF (15 mL) was added, and the mixture stirred for 12 h at room temperature, then the reaction mixture poured into water and extracted with *n*-hexane. The organic

layer was washed with saturated aqueous NH_4Cl and water, and dried over Na_2SO_4. The residue was purified by column chromatography on silica gel by eluting with *n*-hexane, to give **1** as a colorless liquid (2.41 g, 80%). ^{1}H NMR ($CDCl_3$, 400.13 MHz, ppm): δ 6.95 (1H, s, Ar*H*), 2.72 (2H, t, *J* = 7.2 Hz, -C*H*$_2$-), 2.53 (2H, t, *J* = 7.6 Hz, -C*H*$_2$-), 1.57-1.65 (2H, m, -C*H*$_2$-), 1.45-1.52 (2H, m, -C*H*$_2$-), 1.26-1.32 (36H, m, -C*H*$_2$-), 0.88 (6H, t, *J* = 6.4 Hz, -C*H*$_3$). ^{13}C NMR ($CDCl_3$, 100.61 MHz, ppm): δ 140.2, 136.7, 119.1, 112.9, 32.5, 32.1, 30.5, 30.3, 30.2, 30.1, 30.0, 29.9, 29.4, 28.4, 23.3, 14.6.

Attachment of the borate ester

2-(4,4,5,5-Tetramethyl-1,3,2-dioxaborolan-2-yl)-4,5-didodecylthiophene (**2**)[28]: To a solution of 2-bromo-4,5-didodecylthiophene (4.0 g, 8.01 mmol) in THF (100 mL) was added dropwise *n*-butyllithium (1.6 M in hexanes, 6.0 mL, 9.61 mmol) at -78 ºC under an Ar atmosphere, and the mixture stirred for 1 h at the same temperature under an Ar atmosphere. To this reaction mixture was slowly added 2-isopropoxy-4,4,5,5-tetramethyl-1,3,2-dioxaborolane (1.79 g, 9.62 mmol), and the reaction mixture stirred overnight at room temperature. The reaction was quenched by adding a small amount of methanol, and ether added to the mixture. The organic layer was washed with brine, water, dried over Na_2SO_4, and the solvent evaporated. The residue was purified by column chromatography on silica gel by eluting with ethyl acetate/*n*-hexane (1:10 v/v), to give **2** as a colorless liquid (3.17 g, 72%). ^{1}H NMR ($CDCl_3$, 400.13 MHz, ppm): δ 7.37 (1H, s, Ar*H*), 2.73 (2H, t, *J* = 7.2 Hz, -C*H*$_2$-), 2.49 (2H, t, *J* = 7.6 Hz, -C*H*$_2$-), 1.54-1.66 (4H, m, -C*H*$_2$-), 1.26-1.41 (36H, m, -C*H*$_2$-), 1.23 (12H, s, -C*H*$_3$), 0.88 (6H, t, *J* = 6.4 Hz, -C*H*$_3$). ^{13}C NMR ($CDCl_3$, 100.61 MHz, ppm): δ 147.5, 140.0, 139.6, 84.1, 32.4, 32.1, 31.2, 30.2, 30.1, 30.0, 29.9, 29.8, 29.7, 28.6, 28.5, 25.2, 25.1, 23.2, 14.5.

3-(4,4,5,5-Tetramethyl-1,3,2-dioxaborolan-2-yl)-4,5-didodecylthiophene (**3**)[29,30]: To a solution of **1** (1.0 g, 2.00 mmol) in 1,4-dioxane (10 mL) were added bis(pinacolato)diboron (0.762 g, 3.00 mmol), [1,1'-bis(diphenylphosphino)

-ferrocene]dichloropalladium(II), complex with dichloromethane [Pd(dppf)Cl_2·CH_2Cl_2] (0.163 g, 0.200 mmol), and KOAc (0.589 g, 6.00 mmol). The reaction mixture was stirred at 80 ºC for 6 h under an Ar atmosphere, then the reaction quenched by adding water, and extracted with ether. The organic layer was washed with brine and water, dried over Na_2SO_4, and the solvent evaporated. The residue was purified by column chromatography on silica gel by eluting with ethyl acetate/*n*-hexane (1:3 v/v), to give **3** as a colorless liquid (0.480 g, 44%). ^{1}H NMR ($CDCl_3$, 400.13 MHz, ppm): δ 7.65 (1H, s, Ar*H*), 2.69-2.74 (4H, m, -CH_2-), 1.58-1.65 (2H, m, -CH_2-), 1.42-1.50 (2H, m, -CH_2-), 1.29 (12H, s, -CH_3), 1.27-1.37 (36H, m, -CH_2-), 0.88 (6H, t, *J* = 6.4 Hz, -CH_3). ^{13}C NMR ($CDCl_3$, 100.61 MHz, ppm): δ 143.3, 140.0, 134.3, 83.4, 32.6, 32.4, 32.1, 30.3, 30.2, 30.1, 29.9, 29.8, 28.5, 28.5, 28.1, 25.2, 23.2, 14.6.

Suzuki-Miyaura Coupling Reaction[31]

Compound **4**: To a solution of 4,5-dichlorophthalonitrile (90.1 mg, 0.457 mmol) and **2** (1.00 g, 1.83 mmol) in a mixed solvent of toluene (2.0 mL), 1,2-dimethoxyethane (2.0 mL) and H_2O (1.0 mL) were added $Pd(OAc)_2$ (1.03 mg, 4.59 μmol), 2-dicyclohexylphosphino-2',6'-dimethoxybiphenyl (S-Phos) (3.75 mg, 9.13 μmol) and K_3PO_4(0.397 g, 1.83 mmol), and the reaction mixture stirred at 85 °C for 12 h under an Ar atmosphere. After cooling to room temperature, the reaction mixture was poured into water, and extracted with CH_2Cl_2. The organic layer was dried over $MgSO_4$ and the solvent evaporated. The residue was purified by column chromatography on silica gel by eluting with CH_2Cl_2/*n*-hexane (1/1 v/v) and recycling preparative HPLC, to give **4** as a pale yellow oily liquid (0.269 g, 61%). ^{1}H NMR ($CDCl_3$, 400.13 MHz, ppm): δ 7.81 (2H, s, Ar*H*), 6.72 (2H, s, Ar*H*), 2.69 (4H, t, *J* = 7.6 Hz, -CH_2-), 2.43 (4H, t, *J* = 7.2 Hz, -CH_2-), 1.55-1.63 (4H, m, -CH_2-), 1.44-1.49 (4H, m, -CH_2-), 1.26-1.33 (72H, m, -CH_2-), 0.88 (12H, t, *J* = 6.8 Hz, -CH_3). ^{13}C NMR ($CDCl_3$, 100.61 MHz, ppm): δ 143.6, 139.4, 139.3, 135.5, 134.2, 131.2, 115.8, 113.6, 32.6, 32.2, 31.2, 30.2, 30.1, 30.0, 29.9, 29.8, 29.7,

28.5, 28.3, 23.1, 14.5.

Compound **5**: Compound **5** was synthesized from 4,5-dichlorophthalonitrile (66.1 mg, 0.335 mmol) and **3** (0.737 g, 1.35 mmol) by the same procedure as for **4**. Yield 67% (yellow oily liquid). ^{1}H NMR ($CDCl_3$, 400.13 MHz, ppm): δ 7.75 (2H, s, Ar*H*), 6.68 (2H, s, Ar*H*), 2.67 (4H, t, *J* = 7.6 Hz, -C*H*$_2$-), 2.18 (4H, t, *J* = 6.4 Hz, -C*H*$_2$-), 1.58 (4H, t, *J* = 7.2 Hz, -C*H*$_2$-), 1.26-1.37 (76H, m, -C*H*$_2$-), 0.879 (12H, t, *J* = 7.2 Hz, -C*H*$_3$). ^{13}C NMR ($CDCl_3$, 100.61 MHz, ppm): δ 143.4, 141.5, 138.4, 136.1, 135.6, 122.6, 115.8, 114.1, 32.4, 32.2, 31.0, 30.1, 30.0, 29.9, 29.8, 29.7, 29.6, 29.4, 28.7, 27.3, 23.1, 21.7, 14.5.

$FeCl_3$-mediated Oxidative Cyclization[26,27]

Compound **6**: To a CH_2Cl_2 solution (50 mL) of **4** (0.269 g, 0.307 mmol) was added a CH_3NO_2 solution (10 mL) of $FeCl_3$ (0.226 g, 1.39 mmol) at 0 ºC under an Ar atmosphere, and the resulting solution stirred at room temperature for 30 min. The reaction was quenched by adding methanol (25 mL), and an organic extract washed with brine and saturated aqueous NH_4Cl, dried over Na_2SO_4, and the solvent evaporated. The residue was purified by column chromatography on silica gel by eluting with CH_2Cl_2/*n*-hexane (1/1 v/v) and recrystallization from acetone, to give **6** as a pale yellow solid (0.193 g, 72%). ^{1}H NMR ($CDCl_3$, 400.13 MHz, ppm): δ 8.42 (2H, s, Ar*H*), 2.97-3.05 (8H, m, -C*H*$_2$-), 1.75-1.82 (4H, m, -C*H*$_2$-), 1.17-1.46 (76H, m, -C*H*$_2$-), 0.85-0.89 (12H, m, -C*H*$_3$). ^{13}C NMR ($CDCl_3$, 100.61 MHz, ppm): δ 144.5, 137.5, 136.2, 133.8, 130.8, 127.7, 116.6, 109.6, 32.4, 32.0, 30.4, 30.2, 30.1, 30.0, 29.9, 29.8, 29.7, 23.1, 14.5. Melting point (Mp): 53 ºC. IR (ATR): 2228 cm^{-1} (νCN). MALDI-TOF Ms (dithranol): *m/z* 962.08 (M+H, 100%), Calcd. for $C_{64}H_{102}N_2S_2$: *m/z* 962.75. UV-Vis (in CH_2Cl_2): λ (log ε / M^{-1} cm^{-1}) = 336 (4.76) nm.

Compound **7**: Compound **7** was synthesized from **5** (0.216 g, 0.224 mmol) and $FeCl_3$ (0.181 g, 1.12 mmol) by the same procedure as for **6**. Yield 86% (0.185 g). ^{1}H NMR ($CDCl_3$, 400.13 MHz, ppm): δ 8.78 (2H, s, Ar*H*), 3.03 (4H, t, *J* = 6.8 Hz,

-C*H*$_2$-), 2.93 (4H, t, *J* = 7.6 Hz, -C*H*$_2$-), 1.73-1.81 (4H, m, -C*H*$_2$-), 1.26-1.67 (76H, m, -C*H*$_2$-), 0.878 (12H, t, *J* = 7.2 Hz, -C*H*$_3$). ^{13}C NMR ($CDCl_3$, 100.61 MHz, ppm): δ 141.6, 136.2, 134.6, 131.0, 130.5, 129.6, 116.9, 108.6, 32.4, 30.1, 30.0, 29.9, 29.8, 29.7, 29.4, 29.2, 23.1, 14.5. Mp: 57 ºC. IR (ATR): 2228 cm^{-1} (νCN). MALDI-TOF Ms (dithranol): *m/z* 962.28 (M+H, 100%), Calcd. for $C_{64}H_{102}N_2S_2$: *m/z* 962.75. UV-Vis (in CH_2Cl_2): λ (log ε / M^{-1} cm^{-1}) = 285 (4.80), 317 (4.67), 395 (4.03) nm.

*Teteracyclization of **6** and **7***[32,33]

ZnTNc$_{endo}$. A mixture of **6** (100.0 mg, 0.104 mmol), 1,8-diazabicyclo[5.4.0]-7-undecene (DBU) (15.5 μL, 0.104 mmol), $Zn(OAc)_2$ (4.76 mg, 25.9 μmol) in 1-pentanol (1.0 mL) was stirred at 140 °C for 12h under an Ar atmosphere. After cooling to room temperature, the reaction mixture was poured into water and extracted with CH_2Cl_2. The organic layer was washed with water, dried over Na_2SO_4, and the solvent evaporated. The residue was purified by column chromatography on activated alumina by eluting with *n*-hexane and recycling preparative HPLC, to give **ZnTNc$_{endo}$** (51.8 mg, 51%). ^{1}H NMR ($CDCl_3$, 400.13 MHz, ppm): δ 9.33 (8H, brs, Ar*H*), 2.79-3.53 (32H, br, -C*H*$_2$-), 1.28-2.09 (320H, br, -C*H*$_2$-), 0.82-0.89 (48H, br, -C*H*$_3$). MALDI-TOF Ms (dithranol): *m/z* 3914.91 (M+H, 100%), Calcd. for $C_{256}H_{408}N_8S_8Zn$: *m/z* 3914.92. UV-Vis-NIR (in THF): λ (log ε / M^{-1} cm^{-1}) = 363 (5.13), 452 (4.83), 692 (4.84), 740 (4.83), 775 (5.57) nm.

ZnTNc$_{exo}$: **ZnTNc$_{exo}$** was synthesized from **7** (80 mg, 83.0 μmol), DBU (12.4 μL, 20.8 μmol) and $Zn(OAc)_2$ (3.81 mg, 83.0 μmol) by the same procedure as for **ZnTNc$_{endo}$**. Yield 50% (41.0 mg). ^{1}H NMR ($CDCl_3$, 400.13 MHz, ppm): δ 10.86 (8H, brs, Ar*H*), 2.51-4.41 (32H, br, -C*H*$_2$-), 0.48-2.34 (368H, br, -C*H*$_2$-, -C*H*$_3$). MALDI-TOF Ms (dithranol): *m/z* 3914.44 (M+H, 100%), Calcd. for $C_{256}H_{408}N_8S_8Zn$: *m/z* 3914.92. UV-Vis-NIR (in THF): λ (log ε / M^{-1} cm^{-1}) = 353 (5.24), 475 (4.26), 692 (4.85), 739 (4.81), 778 (5.55) nm.

3.2.3 Time-of-flight measurements[34,35]

Measurement cells for TOF were composed of two Indium tin oxide (ITO) patterned glass substrates and a silicon spacer containing silica beads with 15 μm diameter. The effective area of the cells was 0.25 cm^2. Powdered samples of **ZnTNc$_{endo}$** or **ZnTNc$_{exo}$** (ca. 5mg) were put on the bottom ITO substrate, and the cells placed in a vacuum oven. After evacuation, the oven was filled with argon, and heated at 210 or 260 ºC for **ZnTNc$_{exo}$** and **ZnTNc$_{end}$**, respectively. The area between the two ITO electrodes was filled with melted **ZnTNc$_{exo}$** or **ZnTNc$_{endo}$** by injection from the cell slit through capillary action, and the cell was then cooled to room temperature at 1 ºC min^{-1} inside the oven, to achieve the formation of large-area domains. The transient photocurrents were detected using a digital oscilloscope after light irradiation with a 377 nm N_2-pulse laser having a pulse width of 800 ps under various electric fields. An electric field was created in the cell using a DC power supply. The temperature of the cells was controlled within 0.2 K using a temperature controller and a hot stage. Carrier (hole or electron) mobility μ was calculated from the following equation, $\mu = d^2 / (V t_t)$ where d is the sample thickness, V is the applied bias, and t_t is the transit time of the photo-generated carriers traversing the sample layer. The t_t values of the photo-generated carriers in the material were determined from an inflection point on the double logarithmic plot of the transient photocurrent decay curves.

3.3 Results and Discussion

3.3.1 Syntheses of thiophene-fused phthalonitriles

Thiophene-fused ZnNc derivatives were synthesized from 4,5-dithienylphthalonitrile by Yan et al., and they studied their aggregation behavior in solution.[36] In contrast, when the author synthesized a thiophene-fused ZnNc decorated with eight alkyl chains according to this synthetic route, the resulting ZnNc did not show thermotropic liquid crystalline behavior. This suggests that the introduction of eight alkyl chains is insufficient for forming liquid crystalline phases for the large thiophene-fused ZnNc core. Thus, the author designed and synthesized two isomers **ZnTNc$_{endo}$** and **ZnTNc$_{exo}$** possessing sixteen dodecyl chains, in which flexible dodecyl chains were attached to the two positions of the peripheral thiophene rings.

Regioisomers of thiophene-fused phthalonitriles **6** and **7** were synthesized from 2-bromo-4,5-didodecylthiophene as a starting material (Scheme 1). 2-Bromo-4,5-didodecylthiophene was prepared from 3-bromothiophene according to the procedure reported by Kuo et al.[26] Compound **2** was synthesized from 2-bromo-4,5-didodecylthiophene by the selective lithiation at the α-hydrogen of the thiophene ring using *n*-butyllithium, followed by reaction with 2-isopropoxy-4,4,5,5-tetramethyl-1,3,2-dioxaborolane.[28] The other isomer **3** was prepared in two synthetic steps: isomerization of 2-bromo-4,5-didodecylthiophene with lithium diisopropylamide (LDA),[26,27] and the palladium-catalyzed Miyaura borylation reaction with bis(pinacolato)diboron.[29,30] Phthalonitrile precursors **4** and **5** were synthesized by the Suzuki-Miyaura coupling reaction of 4,5-dichlorophthalonitrile with **2** or **3** in the presence of a palladium catalyst using S-Phos ligand.[31] The two thiophenes in **4** and **5** were fused by $FeCl_3$-mediated oxidative cyclization.[26,27] Phthalonitriles **6** and **7**, in which two thiophenes are annealed at different positions, were isolated as yellow solids, and unambiguously

characterized by NMR spectroscopy, FT-IR, and MALDI-TOF mass spectrometry.

***Scheme 1**. Syntheses of **ZnTNc**$_{endo}$ and **ZnTNc**$_{exo}$*[a]

R = *n*-$C_{12}H_{25}$

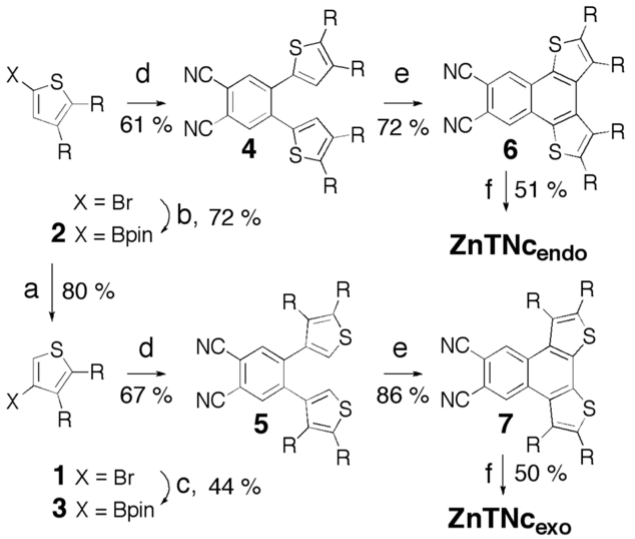

[a] Reagents and conditions: (a) LDA, THF, RT; (b) (i) 1.6 M *n*-BuLi, THF, -78 ºC; (ii) 2-isopropoxy-4,4,5,5-tetramethyl-1.3.2-dioxaborolane, RT; (c) bis(pinacolato)diboron, $Pd(dppf)Cl_2 \cdot CH_2Cl_2$, KOAc, 1,4-dioxane, 80 ºC; (d) 4,5-dichlorophthalonitrile, $Pd(OAc)_2$, S-Phos, K_3PO_4, Toluene, DME, H_2O, 85 ºC; (e) $FeCl_3$, CH_3NO_2, DCM, 0 ºC; (f) $Zn(OAc)_2$, DBU, 1-pentanol, 140 ºC.

3.3.2 Optical properties of precursor phthalonitriles

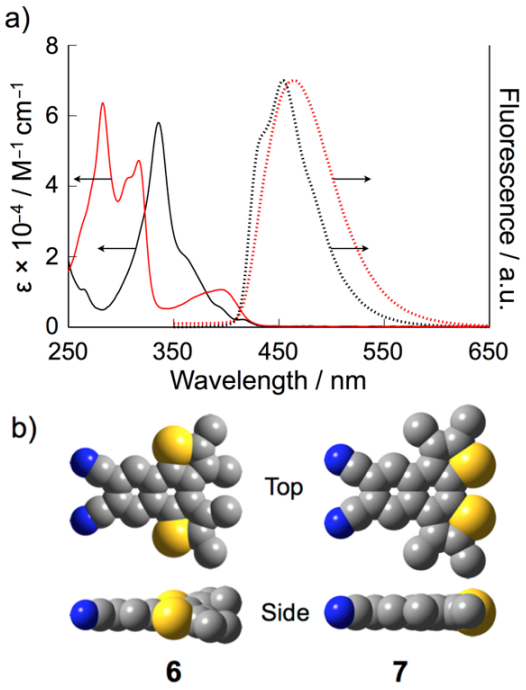

Fig. 1. *a) Absorption and fluorescence spectra of* ***6*** *(black line) and 7 (red line) in* CH_2Cl_2. *b) Optimized structures of* ***6*** *and 7* ***(****methyl-substituted analogues****)*** *obtained by DFT at the B3LYP/6-31G(d) level.*

Fig. 1a shows the absorption and fluorescence spectra of **6** and **7** in CH_2Cl_2. The shapes of the absorption spectra of **6** and **7** were different, and the emission maximum of **7** was red-shifted relative to that of **6**. Density functional theory (DFT) calculations were conducted for **6** and **7**, in order to gain insight into the equilibrium geometries and electronic structures of the frontier orbitals of the compounds. The transitions calculated by time-dependent (TD) DFT agreed well with the experimental absorption spectra of **6** and **7** (Fig. 2). While **7** has a planar geometry, the other isomer **6** shows a less planar structure as shown in Fig. 1b. The steric hindrance arising from the methyl units of two different thiophenes in **7** induces strain in the thiophene-fused phthalonitrile. The differences in the absorption and fluorescence spectra of **6** and **7** can be explained by a change in

conjugation caused by the strain of the aromatic rings.[37]

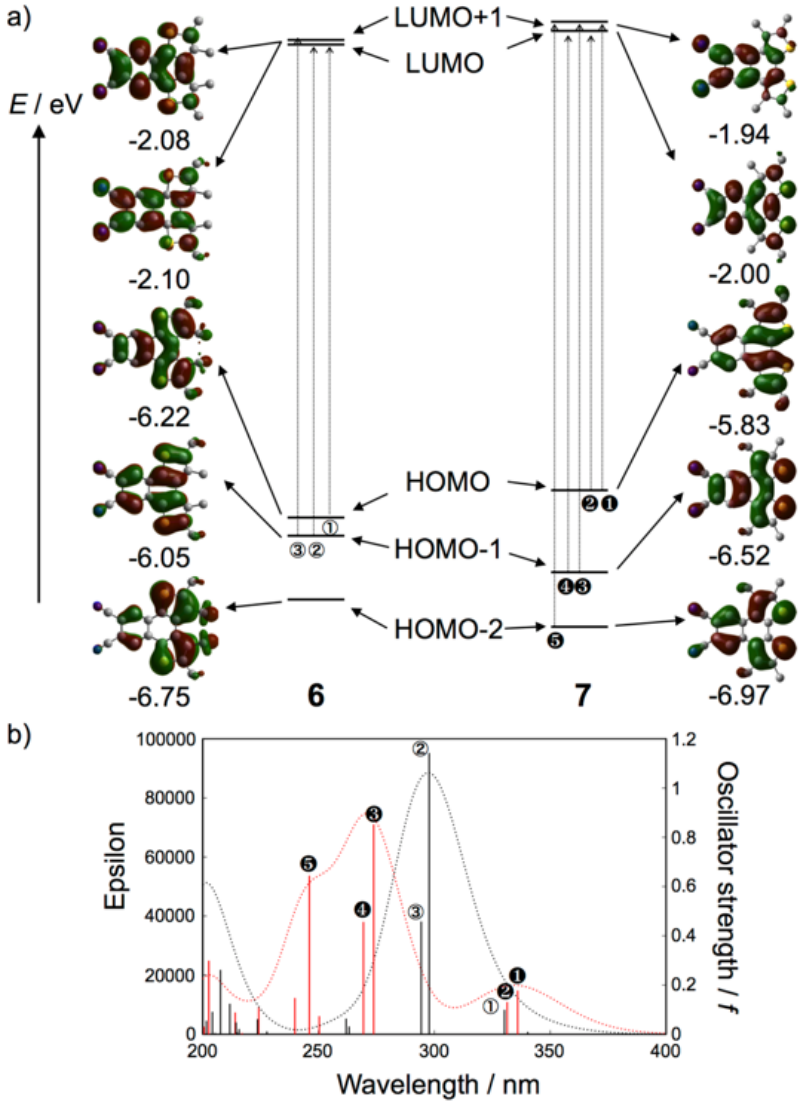

Fig. 2. *a) Molecular orbitals and energy diagrams of* ***6*** *and* ***7*** *(methyl-substituted analogues) obtained by DFT at the B3LYP/6-31G(d) level, respectively. b) Simulated absorption spectra and oscillator strength of* ***6*** *(black) and* ***7*** *(red) obtained by TD-DFT at the CAM-B3LYP/6-31G(d) level.*

3.3.3 Syntheses and optical-electrochemical properties of thiophene-fused zinc naphthalocyanines

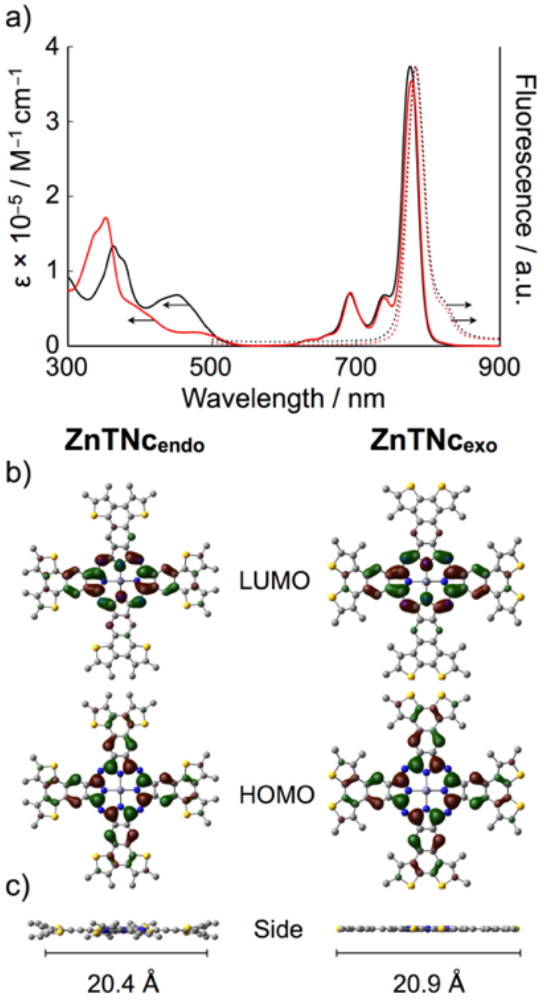

Fig. 3. *a) Absorption and fluorescence spectra of* ***ZnTNc$_{endo}$*** *(black line) and* ***ZnTNc$_{exo}$*** *(red line) in THF. b), c) HOMO/LUMO orbitals and optimized structures of* ***ZnTNc$_{endo}$*** *and* ***ZnTNc$_{exo}$*** *(methyl-substituted analogues) obtained by DFT at the B3LYP/6-31G(d) level.*

The syntheses of **ZnTNc$_{endo}$** and **ZnTNc$_{exo}$** decorated with sixteen alkyl chains were achieved by heating **6** or **7** with DBU and zinc acetate in *n*-pentanol.[32,33] Both complexes were characterized by NMR spectroscopy and MALDI-TOF mass

spectrometry, and were found to be highly soluble in many organic solvents except for acetone and alcohols. Phthalocyanine analogues exhibit a strong absorption band (Q band) in the near IR region, and the Q band position can be shifted to longer wavelength with increasing size of the π-system.[11] However, **ZnTNc$_{endo}$** and **ZnTNc$_{exo}$** showed sharp Q bands at 775 and 778 nm in THF (Fig. 3a and Table 1), and the positions of the Q band in **ZnTNc$_{endo}$** and **ZnTNc$_{exo}$** are equal to that of zinc(II) tetra(*tert*-butyl)naphthalocyanine (Zn(*t*-Bu)Nc) lacking fused thiophene rings (λ_{max} = 778 nm).[38] The fluorescence spectra of **ZnTNc$_{endo}$** and **ZnTNc$_{exo}$** have a peak at 783 nm with a near mirror image of the Q band and a very small Stoke-shift. The optical HOMO-LUMO band-gaps (E_g) for **ZnTNc$_{endo}$** and **ZnTNc$_{exo}$** were determined to be 1.6 eV from the crossing point of the normalized absorption and fluorescence spectra. The electron density distributions of the HOMO and LUMO calculated by DFT are mainly populated over the Nc skeleton within **ZnTNc$_{endo}$** and **ZnTNc$_{exo}$** (Fig. 3b and 4). While the Q band position of phthalocyanine can be shifted to the near-IR by linear annulation, to form Nc and further to anthracocyanine, the angular annulation does not result in a red-shift of the Q band.[11,39] The fusing of thiophene rings at the angular positions of Nc in **ZnTNc$_{endo}$** and **ZnTNc$_{exo}$** does not effect a shift of the Q band as well as the change of E_g.

According to the equilibrium geometries calculated by DFT (Fig. 3c), the peripheral two thiophene rings in **ZnTNc$_{endo}$** are twisted, due to the steric repulsion of neighboring alkyl groups. The molecular dimensions of **ZnTNc$_{endo}$** and **ZnTNc$_{exo}$** were estimated from the analysis of the surface pressure versus area (π-A) isotherm on pure water as the subphase (Fig. 5).[40] The limiting surface areas per molecule of **ZnTNc$_{endo}$** and **ZnTNc$_{exo}$** were estimated to be 1.47 and 1.10 nm^2, determined by extrapolating the slope of the π-A isotherm in the liquid-condensed region to zero pressure. The observed area of **ZnTNc$_{endo}$** was larger than that of **ZnTNc$_{exo}$**, suggesting a larger stacking distance between the thiophene-fused Nc

rings within the edge-on stacks on water by distortion of the structure from planarity in **ZnTNc$_{endo}$**.

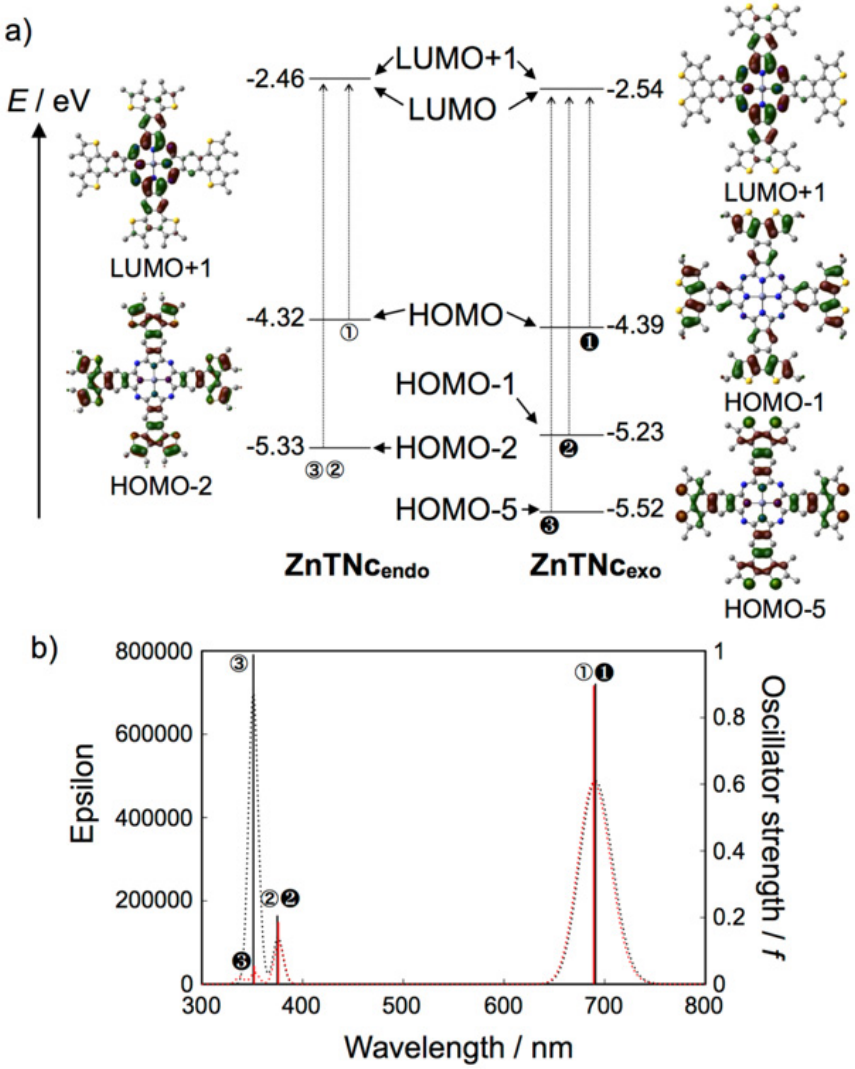

Fig. 4. *a) Molecular orbitals and energy diagrams of* ***ZnTNc$_{endo}$*** *and* ***ZnTNc$_{exo}$*** *(methyl-substituted analogues) obtained by DFT at the B3LYP/6-31G(d) level, respectively. b) Simulated absorption spectra and oscillator strength of* ***ZnTNc$_{endo}$*** *(black) and* ***ZnTNc$_{exo}$*** *(red) obtained by TD-DFT at the CAM-B3LYP/6-31G(d) level.*

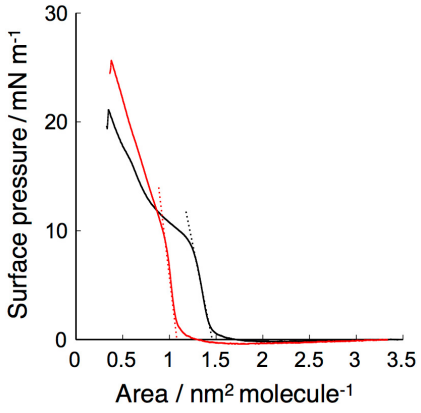

Fig. 5. *Surface pressure vs. area per molecule isotherms for* ***ZnTNc$_{endo}$*** *(black line) and* ***ZnTNc$_{exo}$*** *(red line) on triply distilled water at 25 ºC.*

The HOMO energy levels of **ZnTNc$_{endo}$** and **ZnTNc$_{exo}$** were determined from the first oxidation potential (E_{ox}) by differential pulse voltammetry measurements in dry dichloromethane containing 0.1 M *n*-Bu_4NClO_4 as a supporting electrolyte. Both complexes exhibited one oxidation peak for the oxidation of the Nc ring (ZnNc(-1)/ZnNc(-2)) at -0.02 and -0.15 V *vs*. the ferrocene/ferrocenium couple (Fc/Fc^+), which were negative relative to the E_{ox} of Zn(*t*-Bu)Nc (Table 1).[38] The HOMO energy levels of **ZnTNc$_{endo}$** and **ZnTNc$_{exo}$** were estimated to be -4.8 and -4.7 eV from E_{ox} calibrated by the Fc/Fc^+ redox potential *vs*. vacuum. The HOMO and LUMO energy levels of **ZnTNc$_{endo}$** and **ZnTNc$_{exo}$** were lower than those of Zn(*t*-Bu)Nc, indicating that the fusing of thiophene rings with the Nc ring leads to the stabilization of HOMO and LUMO energy levels.[38]

Table 1*. Photochemical, Electrochemical and Thermal analysis data of* ***ZnTNc$_{endo}$*** *and* ***ZnTNc$_{exo}$****.*

	λ_{abs} [a] (nm)	$\varepsilon_{max} \times 10^{-5}$ (M^{-1} cm^{-1})	λ_{fl} [a] (nm)	E_g^{opt} [b] (eV)	HOMO [c] (eV)	LUMO [c] (eV)	T [ΔH] [d] (ºC[kJmol^{-1}])	T_d [e] (ºC)
ZnTNc$_{endo}$	775	3.72	783	1.6	-4.8	-3.2	-5.5[8], 257[6]	259
ZnTNc$_{exo}$	778	3.55	782	1.6	-4.7	-3.1	5.1[16], 204[12]	245

[a] Measured in THF. [b] Estimated from cross point of normalized absorption and fluorescence spectra. [c] HOMO and LUMO energy levels were determined by HOMO = -(4.8 + $E_{ox}^{1/2}$ (*vs.* Fc/Fc$^+$) and LUMO = HOMO + E_g^{opt}. [d] Phase transition temperatures and their enthalpies determined by DSC. [e] Temperature of starting weight loss determined by TGA.

3.3.4 Liquid crystal properties

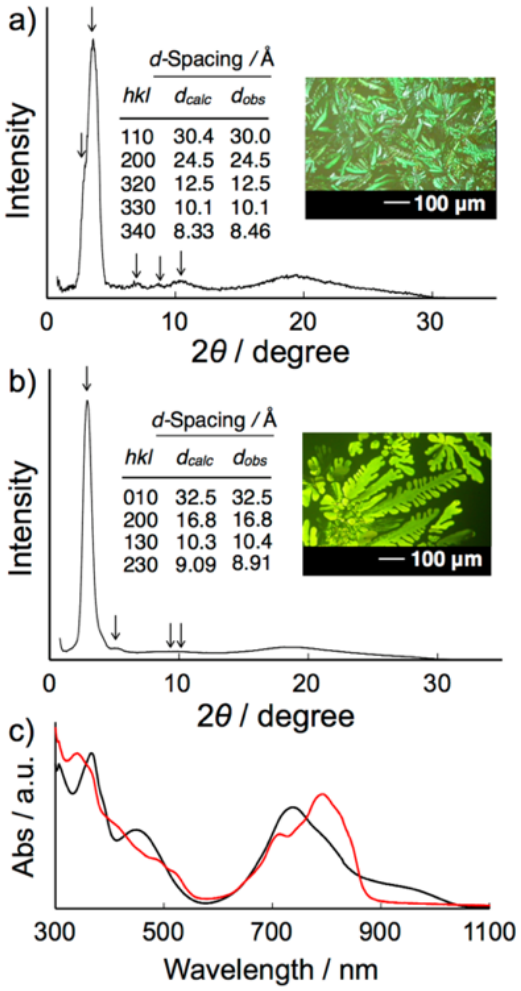

Fig. 6. *X-ray diffraction patterns of a)* ***ZnTNc$_{exo}$*** *at 100 ºC and b)* ***ZnTNc$_{endo}$*** *at 160 ºC. The insets show crossed polarized optical micrographs of* ***ZnTNc$_{exo}$*** *at 190 ºC and* ***ZnTNc$_{endo}$*** *at 240 ºC, and d-spacing values for* ***ZnTNc$_{exo}$*** *and* ***ZnTNc$_{endo}$***. *c) Absorption spectra of* ***ZnTNc$_{endo}$*** *(black line) and* ***ZnTNc$_{exo}$*** *(red line) in their liquid crystalline states on quartz plates.*

The thermal phase transition behavior of **ZnTNc$_{endo}$** and **ZnTNc$_{exo}$** was investigated by a combination of differential scanning calorimetry (DSC) and temperature-controlled polarizing optical microscopy (TPOM). The DSC profile of **ZnTNc$_{exo}$** showed two reversible transitions at 5 and 204 ºC upon heating (Table 1).

In thermogravimetric analysis (TGA) curves, **ZnTNc$_{exo}$** exhibited an onset of weight loss above 240 ºC, suggesting that decomposition does not occur at the transition point, as observed in the DSC (Fig. 7).

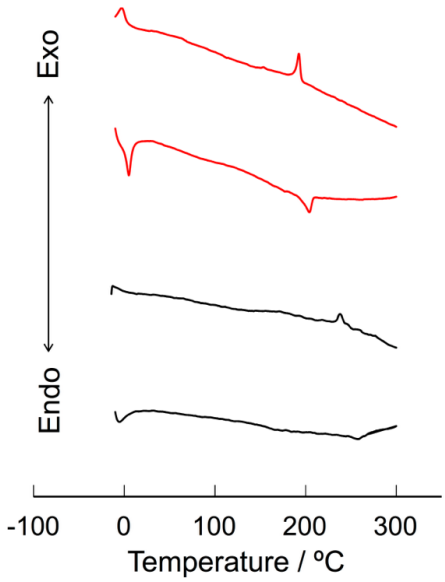

Fig. 7. *DSC profiles for* ***ZnTNc$_{endo}$*** *(black line) and* ***ZnTNc$_{exo}$*** *(red line) at scan rate of 10 ºC/ min.*

Under TPOM, a birefringent dendritic texture appeared at 190 ºC on cooling from the isotropic melt, and remained without any change until room temperature (Fig. 6a). This texture is typical of columnar liquid crystalline materials.[41,42] To confirm the self-organized structure of **ZnTNc$_{exo}$** in the liquid crystalline state, temperature-controlled X-ray diffraction (XRD) measurements were performed. The XRD profile of **ZnTNc$_{exo}$** at 100 ºC revealed a set of diffraction peaks corresponding to a *d* spacing of 30.0, 24.5, 12.5, 10.1, and 8.46 Å, which were indexed in sequence as (100), (200), (320), (330), and (340) of a rectangular columnar (Col_r) lattice with lattice parameters of a = 49.0 and b = 38.7 Å, and with the number of molecules in the unit cell Z = 2. The rectangular lattice has a $P2_1/a$ symmetry, as shown in Fig. 8a. Moreover, the XRD profile in the wide angle

region showed only a broad halo around d = 4.6 Å, and did not exhibit reflections corresponding to the stacking periodicity in the columnar assemblies. While the other isomer **ZnTNc$_{endo}$** also exhibited a columnar liquid crystalline phase, the transition temperature of **ZnTNc$_{endo}$** from the liquid crystalline state to the isotropic melt was 53 ºC higher than that of **ZnTNc$_{exo}$**. The texture of **ZnTNc$_{endo}$** in the liquid crystalline state under TPOM was also different from **ZnTNc$_{exo}$** (Fig. 6b). The XRD reflections of **ZnTNc$_{endo}$** were fitted to a two-dimensional Col$_r$ lattice with *P*2m symmetry (Fig. 8b).

Fig. 6c shows UV-Vis spectra of thin films of **ZnTNc$_{exo}$** and **ZnTNc$_{endo}$** in the liquid crystalline state on quartz plates. UV-Vis spectra provide information on the type of aggregated structures, such as face-to-face, edge-to-edge, and herringbone arrangements.[43,44] The maximum of the Q band for the film of **ZnTNc$_{endo}$** in the liquid crystalline phase was found to be 737 nm, and the blue shift of the Q band compared to the solution spectrum indicates the formation of stacks having a face-to-face arrangement. On the other hand, the **ZnTNc$_{exo}$** film showed a red shift of the Q band position relative to the solution spectrum, suggesting that the aromatic planes in **ZnTNc$_{endo}$** were stacked in an eclipsed conformation within the one-dimensional stacks (Fig. 8a).

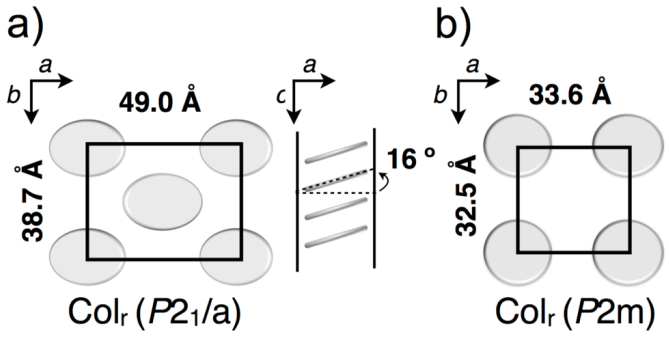

Fig. 8. *Schematic illustrations of two-dimensional columnar packing symmetry and one-dimensional molecular stacking feature of a)* ***ZnTNc$_{exo}$*** *and b)* ***ZnTNc$_{endo}$****.*

The tilted angle of the aromatic plane of **ZnTNc$_{exo}$** in the stacks was estimated to be 16 degrees from the horizontal axis, based on the lattice parameters in the XRD analysis and the molecular dimensions from the DFT calculations. Liquid crystalline Pc and benzoporphyrins substituted with alkyl chains at the lateral positions also showed an eclipsed conformation with a tilt angle to the columnar axis.[45-47] The lateral alkyl chains located at the crowded bay areas of **ZnTNc$_{exo}$** reduce the strength of intermolecular interactions between the aromatic cores due to the steric repulsion of alkyl chains arranged out of the core plane. Recently, Aida and coworkers reported liquid crystalline behavior of propeller-shaped fused oligothiophenes.[27] They found the formation of long-range columnar assemblies of oligothiophenes through well-organized intermolecular sulfur-sulfur contacts. The transition enthalpy of **ZnTNc$_{exo}$** from the Col$_r$ to the isotropic phase was larger than that of **ZnTNc$_{endo}$**. The peripheral sulfur atoms in **ZnTNc$_{exo}$** can interact with the other molecules in the neighboring column, and the sulfur-sulfur interaction may stabilize the intercolumnar assemblies in the Col$_r$ phase. However, the author does not have data to support the formation of intermolecular sulfur-sulfur interactions at this stage. A detailed structural analysis of the columnar packing of **ZnTNc$_{exo}$** is currently underway.

The well-organized columnar nanostructures made from liquid crystalline π-conjugated polyaromatic materials can create long-range pathways for mobile charge carriers.[49] The carrier mobilities of liquid crystalline materials have been measured by time-of-flight (TOF) and radiolysis-time resolved microwave conductivity.[50-53] The TOF method gives mobilities of more than micrometer-scale distance in bulk materials. To evaluate the mobilities of **ZnTNc$_{exo}$** and **ZnTNc$_{endo}$**, TOF measurements have been performed for **ZnTNc$_{exo}$** and **ZnTNc$_{endo}$** in the liquid crystalline states. Since the onset of the thermal decomposition of **ZnTNc$_{endo}$** is very close to the melting point, the carrier mobility μ of **ZnTNc$_{endo}$** could not be obtained because of the decomposition during the preparation of

measurement cell. In contrast, the other isomer **ZnTNc$_{exo}$** showed transient photocurrents in the Col$_r$ phase of **ZnTNc$_{exo}$** at 50 and 150 ºC under different applied biases at ±65 and ±80 V. Compound **ZnTNc$_{exo}$** exhibited an ambipolar carrier transport behavior (Fig. 9).

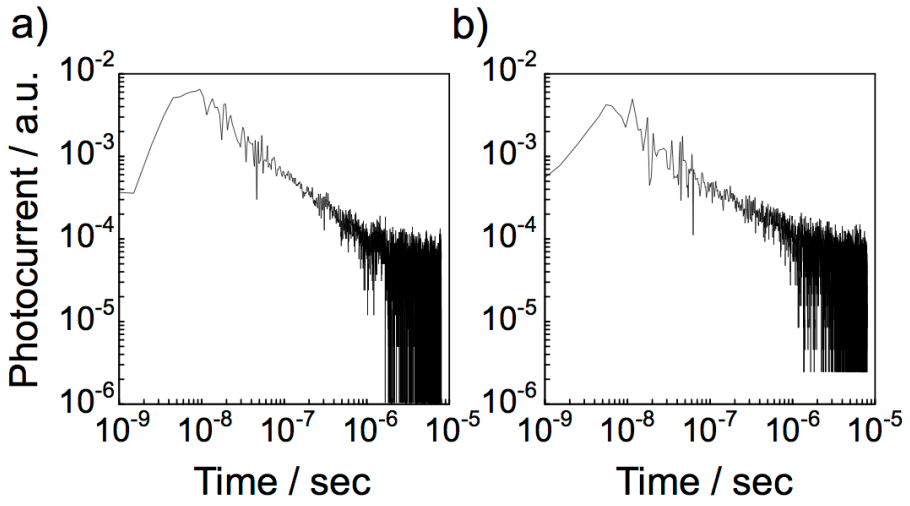

Fig. 9. *Photocurrent decay properties for a) positive (bias voltage = -80 V) and b) negative (bias voltage = 80 V) charge carriers of* ***ZnTNc$_{exo}$*** *at 150 ºC.*

The hole and electron mobilities are calculated to be 7×10^{-2} and 8×10^{-2} cm^2 V^{-1} s^{-1}, and the mobilities are independent of electrical field as well as temperature. This behavior is a characteristic property often seen for ordered columnar liquid crystalline semiconductors.[48,54] On the other hand, it is known that carrier mobilities are strongly dependent on applied electrical fields in disordered materials in which hopping sites are distributed spatially energetically.[55] Because **ZnTNc$_{exo}$** formed multidomains with imperfect alignment of columns between two electrodes, the hole and electron mobilities of **ZnTNc$_{exo}$** are slightly lower than the reported values of liquid crystalline Pcs. The enlargement of the π-conjugated core and the formation of well-defined nanostructures enhanced the carrier mobilities.[56]

3.4 Conclusion

In conclusion, the author has designed and synthesized two structural regioisomers of near-IR light absorbing **ZnTNc$_{exo}$** and **ZnTNc$_{endo}$** decorated with sixteen long alkyl chains. the author has elucidated the influence of the molecular structural differences in the two isomers on their self-organizing behavior and photoconductivity. Ring-expanded **ZnTNc$_{exo}$** and **ZnTNc$_{endo}$** assemble into one-dimensional columnar nanostructures over a wide temperature range from room temperature. TOF experiments have revealed that the organized **ZnTNc$_{exo}$** shows a well-balanced ambipolar carrier transport behavior, with carrier mobilities of the order of 10^{-2} cm^2 V^{-1} s^{-1}. Spontaneous alignment of columnar assemblies on substrates is a key issue for improving the carrier mobilities. Work is underway in our laboratory to control the columnar alignment on the substrate by structural elaboration of thiophene-fused naphthalocyanines.

3.5 References

1. Berreshim AJ, Müller M and Müllen K. *Chem. Rev.* 1999; **99**: 1747.
2. Wu J, Pisula W and Müllen K. *Chem. Rev.* 2007; **107**: 718.
3. Li C, Liu M, Pshirer NG, Brumgarten M and Müllen K. *Chem. Rev.* 2010; **110**: 6817.
4. Laschat S, Baro A, Steinke N, Giesselmann F, Hägele C, Scalia G, Judele R, Kapatsina E, Sauer S, Schreivogel A and Tosoni M. *Angew. Chem. Int. Ed.* 2007; **46**: 4832.
5. Kumar S. *Chem. Soc. Rev.* 2006; **35**: 83.
6. Claessens CG, Hahn U and Torres T. *Chem. Rec.* 2008, **8**, 75.
7. Kadish KM, Smith KM and Guilard R. *The Porphyrin Handbook*, Vol. 15-20, Academic press: San Diego, CA, 2003.
8. Piechicki C, Simon J, Skoulios A, Guillon D and Weber P. *J. Am. Chem. Soc.*

1982; **104**: 5245.

9. Melville OA, Lessard BH and Bender TP. *ACS Appl. Mater. Interfaces*. 2015, **7**, 13105.
10. Dao QD, Hori T, Fukumura K, Masuda T, Kamikado T, Fujii A, Shimizu Y and Ozaki M. *Appl. Phys. Lett.* 2012; **101**: 263301.
11. Kobayashi N, Nakajima S, Ogata H and Fukuda T. *Chem. Eur. J.* 2004; **10**: 6294.
12. Fox JM, Katz TJ, Elshocht SV. Verbiest T, Kauranen M, Persoons A, Thongpanchang T, Krauss T and Brus L. *J. Am. Chem. Soc.* 1999; **121**: 3453.
13. Maya EM, Snow AW, Shirk JS, Flom SR, Pong RGS and Callahan JH. *J. Porphyr. Phthalocyanines* 2002; **6**: 463.
14. Sooksimuang T and Mandal BK. *J. Org. Chem.* 2003; **68**: 652.
15. Chen LX, Shaw GB, Tiede DM, Zuo X, Zapol P, Redfern PC, Curtiss LA, Sooksimuang T and Mandal BK. *J. Phys. Chem. B* 2005; **109**: 16598.
16. Cammidge AN and Gopee H, *Chem. Eur. J.* 2006; **12**: 8609.
17. Fogel Y, Kastler M, Wang Z, Andrienko D, Bodwell GJ and Müllen K. *J. Am. Chem. Soc.* 2007; **129**: 11743.
18. Zöphel L, Mail KS, Reddy PS, Wagner M, de Feyter S, Pisula W and Müllen K. *Chem. Eur. J.* 2012; **18**: 3264.
19. Ng DKP, Yeung Y-O, Chan WK and Yu S-C. *Tetrahedron Lett.*, **1997**, 38, 6701.
20. Cammidge AN and Gopee H. *Chem. Commun.*, **2002**, 966-967.
21. Zhang Y, Pan N, Xue Q. Bai M and Jiang J. *J. Porphyr. Phthalocyanines* 2006; **10**: 1132.
22. Ichihara M, Miida M, Mohr B and Ohta K. *J. Porphyr. Phthalocyanines* 2006; **10**: 1145.
23. Wang C, Dong H, Hu W, Liu Y and Zhu D. *Chem. Rev.* 2012; **112**: 2208.
24. Cinar ME and Ozturk T. *Chem. Rev.* 2015; **115**: 3036.
25. Kuo C-Y, Nie W, Tsai H, Yen H-J, Mohite AD, Gupta G, Dattelbaum AM, William DJ, Cha KC, Yang Y, Wang L and WangH-L. *Macromolecules* 2014; **47**: 1008.
26. Brusso JL, Hirst OD, Dadvand A, Ganesan S, Cicoira F, Robertson CM,

Oakley T, Rosei F and Perepichka DF. *Chem. Mater.* 2008; **20**: 2484.

27. Xiao Q, Sakurai T, Fukino T, Akaike K, Honsho Y, Saeki A, Seki S, Tanaka M and Aida T. *J. Am. Chem. Soc.* 2013; **135**: 18268.
28. Muroga T, Sakaguchi T and Hashimoto T. *Polymer* 2012; **53**: 4380.
29. Ishiyama T, Murata M and Miyaura N. *J. Org. Chem.* 1995; **60**: 7508.
30. Sonar P, Singh SP, Lecler P, Surin M. Lazzaroni R, Lin TT, Dodabalapur A and Sellinger A. *J. Mater. Chem*. 2009; **19**: 3228.
31. Martin R and Buchwald SL. *Acc. Chem. Res*. 2008; **41**: 1461.
32. Wöhrle D, Schnurpfeil G and Knothe G. *Dyes Pigm.* 1992; **18**: 91.
33. Poon K-W, Liu W, Chan P-K, Yang Q, Chan T-WD, Mak TCW and Ng DKP. *J. Org. Chem.* 2001; **66**: 1553.
34. Scher H and Montroll EW. *Phys. Rev. B* 1975; **12**: 2455.
35. Hayashi H, Nihashi W, Umeyama T, Matano Y, Seki S, Shimizu Y and Imahori H. *J. Am. Chem. Soc*. 2011; **133**: 10736.
36. Yan X, Fan H, Gu H, Zhang J, Huang X, Zhang R and Zhan X. *Dyes Pigm.* 2015; **114**: 124.
37. Nenajdenko VG, Balenkova ES, Chernichenko KY and Vshivenko SS. *Russ. Chem. Bull. Int. Ed*. 2012; **61**: 1456.
38. Maligaspe E, Kumpulainen T, Lemmetyinen H, Tkachenko NV, Subbaiyan NK, Zandler ME and d'Souza F, *J. Phys. Chem. A* 2010; **114**: 268.
39. Ortí E, Piqueras EC, Crespo R and Brédas JL. *Chem. Mater.* 1990; **2**: 110.
40. Tieke B. *Adv. Mater.* 1990; **2**: 222.
41. Zniber R, Achour R, Cherkaoui MZ, Donnio B, Gehringer L and Guillon D. *J. Mater. Chem*. 2002; **12**: 2208.
42. Sakurai T, Shi K, Sato H, Tashiro K, Osuka A, Saeki A, Seki S, Tagawa S, Sasaki S, Masunaga H, Osaka K, Takata M and Aida T. *J. Am. Chem. Soc.* 2008; **130**: 13812.
43. Ohta K, Azumane S, Kawahara W, Kobayashi N and Yamamoto I. *J. Mater. Chem*. 1999; **9**: 2313.
44. Snow AW. *The Porphyrin Handbook*, Vol 17, Kadish KM, Smith KM and Guilard R. (Eds.) Academic press: San Diego, CA, 2003; pp 129.
45. Iino H, Hanna J, Bushby RJ, Movaghar B, Whitaker BJ and Cook MJ. *Appl.*

Phys. Lett. 2005; **87**: 132102.

46. Miyake Y, Shiraiwa Y, Okada K, Monobe H, Hori T, Yamasaki N, Yoshida H, Cook MJ, Fujii A, Ozaki M and Shimizu Y. *Appl. Phys. Express*. 2011; **4**: 021604.
47. Tate DJ, Anémian R, Bushby RJ, Nanan S, Warriner SL and Whitaker BJ. *Beilstein J. Org. Chem*. 2012; **8**: 120.
48. Liu Z-Y, Usui T, Iino H and Hanna J. *J. Mater. Chem. C* 2013; **1**: 8186.
49. Adam D, Schuhmacher P, Simmerer J, Häussling L, Siemensmeyer K, Etzbachi KH, Ringsdorf H and Haarer D. *Nature* 1994; **371**: 141.
50. Eichhorn H. *J. Porphyr. Phthalocyanines* 2000; **4**: 88.
51. Warman JM, Kroeze JE, Schouten PG and van de Craats AM. *J. Porphyr. Phthalocyanines* 2003; **7**: 342.
52. Bushby RJ and Lozman OR. *Curr. Opin. Solid State Mat. Sci*. 2002; **6**: 569.
53. Pisula W, Zorn M, Chang JY, Müllen K and Zentel R. *Macromol. Rapid Commun*. 2009; **30**: 1179.
54. Donovan KJ, Kreouzis T. *J. Appl. Phys*. 2000; **88**: 918.
55. van de Auweraer M, Schryver FC, Borsenberger PM, Bässler H. *Adv. Mater*. 1994; **6**: 199.
56. van de Craats AM and Warman JM. *Adv. Mater*. 2001; **13**: 130.

Chapter 4

Supramolecular complex formation of resorcin [4]arene-modified zinc phthalocyanine and fullerene

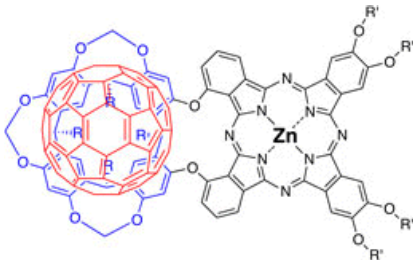

Abstract

A resorcin[4]arene-strapped zinc phthalocyanine **1**, in which two benzene rings of the upper rim of resorcin[4]arene were fused to the adjacent phthalocyanine ligand, was synthesized from two phthalonitriles. Introducing resorcin[4]arene on one side of zinc phthalocyanine strongly affects the spectroscopic property of the phthalocyanine. The Q-band of **1** in CH_2Cl_2 is split into 694 and 740 nm due to the self-protonation of **1** on the *meso*-nitrogen of phthalocyanine ligand. Bowl-shaped resorcin[4]arene can capture C_{60} through the non-covalent interactions, and the complexation between **1** and C_{60} results in an efficient photo-induced electron transfer.

4.1 Introduction

For the past two decades, much attention has been focused on the construction of supramolecular functional systems consisting of functional molecular components.[1,2] The components are correctly oriented with respect to one another and interact in a well-defined intercomponent relationship. Fullerenes and π-conjugated macrocycles such as porphyrins and phthalocyanines have been utilized as important molecular components for the design of artificial photosynthesis and solar energy conversion, and a number of donor-acceptor (D-A) dyads have been designed and synthesized through covalent linkages or non-covalent assemblies between π-conjugated macrocycles and C_{60}.[3-8] Porphyrins and phthalocyanines in the dyads acted as electron donors as well as a light-harvesting antenna in the visible light region. Fullerenes have been employed as electron acceptors to exhibit efficient electron transfer properties in the D-A dyad systems. The spatial arrangements of components in the D-A dyads affected the charge separated lifetimes after an intermolecular electron transfer from π-conjugated macrocycles to C_{60}.[3-8]

Bowl shaped calixarenes and resorcinarenes are versatile frameworks of molecular hosts for guest molecules.[9] These hosts can form stable supramolecular complexes with fullerenes because the recognition sites in the hosts are pre-organized in the hydrophobic cavity to favorably surround a spherical fullerene guest.[9-11] The author expected that introducing bowl shaped hosts to a photoactive zinc phthalocyanine would lead to a supramoelcular electron-transfer system with C_{60} through the non-covalent capturing of C_{60} within the host cavity.[12-15]

This chapter reports the synthesis of resorcin[4]arene-strapped zinc phthalocyanine **1** and the formation of a supramolecular complex between **1** and C_{60} in toluene.

4.2 Experimental section

4.2.1 General procedures

NMR spectra were recorded on a Bruker AVANCE 400 FT NMR spectrometer at 399.65 MHz and 100.62 MHz for ^{1}H and ^{13}C in $CDCl_3$ solution. Chemical shifts are reported relative to internal TMS. IR spectra were obtained on a SHIMAZU IR Prestige-21 with DuraSample IR II. UV-Vis spectra and fluorescence spectra were measured on a JASCO V-650 and a JASCO FP-750. MALDI-TOF mass spectra were obtained on a Bruker autoflex spectrometer with dithranol as matrix.

All chemicals were purchased from commercial suppliers and used without purification. The partially bridged resorcin[4]arene **2** and the phthalonitrile **4** were synthesized according to the reported procedure.[24,33] Column chromatography was performed with activated alumina (Wako, 200 mesh) or silica gel (Wakogel C-200). Recycling preparative gel permeation chromatography was carried out by a JAI recycling preparative HPLC using $CHCl_3$ as an eluent. Analytical thin layer chromatography was performed with commercial Merck plates coated with silica gel 60 F_{254} or aluminum oxide 60 F_{254}.

4.2.2 Syntheses

3: Potassium carbonate (0.5g, 3.50mmol), 3-nitrophthalonitrile (0.18g, 1.05mmol), and **2** (0.4g, 0.35mmol) were stirred in dry DMF (5 ml) at room temperature under a nitrogen atmosphere for one night. The reaction mixture was poured into water (50 ml), and the aqueous layer was extracted with CH_2Cl_2. After being dried over with $MgSO_4$, the organic layer was evaporated, and the residue was purified by column chromatography (silica gel, eluent: CH_2Cl_2, R_f = 0.1) and preparative recycle HPLC. Yield 0.2g (42%). ^{1}H NMR ($CDCl_3$, 400.13MHz): δ (ppm) = 7.62 (t,

J = 7.6 Hz, 2H, Ar*H*), 7.50 (s, 2H, Ar*H*), 7.31 (s, 2H, Ar*H*), 7.25 (d, *J* = 8.0 Hz, 2H, Ar*H*), 7.12 (d, *J* = 8.0 Hz, 2H, Ar*H*), 6.53 (s, 2H, Ar*H*), 6.32 (s, 2H, Ar*H*), 5.71-5.74 (m, 6H, -OCH_2O-), 4.75 (s, 4H, Ar-C*H*-Ar), 2.17-2.31 (m, 8H, -ArCH_2-), 1.23-1.28 (m, 72H, -CH_2-), 0.88 (t, *J* = 6.4 Hz, 12H, -CH_3). ^{13}C NMR ($CDCl_3$, 100.61MHz): δ (ppm) =159.8, 156.0, 155.2, 154.6, 151.1, 138.5, 137.2, 134.6, 132.1, 128.2, 124.1, 123.7, 120.2, 117.6, 116.8, 114.9, 112.6, 107.8, 99.6, 33.9, 33.4, 31.9, 30.2, 29.8, 27.9, 22.7, 14.1. IR (ATR): ν (cm^{-1}) = 2249 (-CN). MALDI-TOF Ms (dithranol): *m/z* 1394.09 (M+H), Calcd for $C_{91}H_{116}N_4O_8$: *m/z* 1393.92.

1: A mixture of **3** (0.15 g, 0.11 mmol), **4** (0.14g, 0.32 mmol), $ZnCl_2$ (7.3 mg, 53.8 mmol) in DMAE (4 mL) was heated at 150 °C with stirring for 6 h. After the mixture was cooled, the solvent was removed and washed with methanol several times to remove excess Zn ion. The residue was purified by column chromatography on activated alumina (eluent: CH_2Cl_2) and recycling preparative HPLC to give **1**. Yield: 60 mg (24%). ^{1}H NMR ($CDCl_3$, 400.13MHz): δ (ppm) = 8.71-9.46 (m, 6H, Ar*H*), 7.31-7.98 (m, 10H, Ar*H*), 6.52 (s, 2H, Ar*H*), 5.73-5.76 (m, 6H, -OCH_2O-), 4.56-4.70 (m, 12H, Ar-C*H*-Ar, -OCH_2-), 0.85-2.35 (m, 168H, -ArCH_2-, -CH_2-, -C*H*-, -CH_3). MALDI-TOF Ms (dithranol): *m/z* 2337.26 (M+H), Calcd for $C_{147}H_{204}N_8O_{12}Zn$: *m/z* 2337.49. UV-Vis (THF): λ_{max} (log ε) = 686 (5.21), 618 (4.45), 355 (4.76).

4.3 Results and Discussion

4.3.1 Synthesis of resorcin[4]arene-strapped Zinc Phthalocyanine

Scheme 1. *Syntheses of side-strapped ZnPc* ***1***

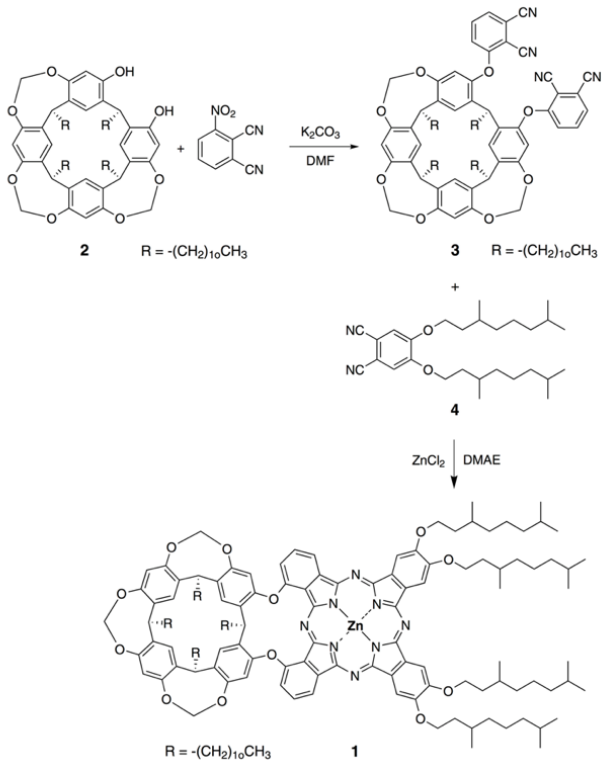

Low-symmetry AABB-type Zinc phthalocyanine (ZnPc) **1** attached with one resorcin[4]arene cavity was prepared from two phthalonitriles **3** and **4**, as shown in Scheme 1.[16-18] The phthalocyanine ring in **1** is strapped with resorcinarene as a bridging group at 1 and 25 positions. The side-strapped Pcs have been synthesized by using bisphthalonitriles bridged at the 3-position.[19-22] In this study, the author prepared a new bisphthalonitrile **3**, in which two phthalonitriles were introduced at the upper rim of resorcin[4]arene through the nucleophilic aromatic substitution reaction between 3-nitrophthalonitrile and a partially bridged resorcin[4]arene **2**.

The partially bridged resorcin[4]arene **2** was synthesized according to the reported procedure.[23,24] The remaining two hydroxyl groups at the upper rim of **2** reacted with 3-nitrophthalonitrile in the presence of K_2CO_3 to give cavitand **3** in 42%. Long alkyl chains were introduced at the lower rim of **3** to improve the solubility in organic solvents.

Cavitand ZnPc **1** was prepared using a mixed tetracyclization of **3** and **4** in a 1:3 molecular ratio in the presence of $ZnCl_2$ in 2-(dimethylamino)ethanol (DMAE) in 24 % yield (scheme 1). The required AABB-type ZnPc **1** was separated by column chromatography and preparative HPLC. ZnPc **1** was characterized by MALDI-TOF mass spectrometry and ^{1}H NMR spectroscopy. Two benzene rings on one side of phthalocyanine ligand were strapped with resorcin[4]arene, and the other two benzene rings were decorated with four branched alkoxy chains. The compound **1** exhibits good solubility in organic solvents such as THF, toluene, CH_2Cl_2 and *n*-hexane.

4.3.2 Cavitand property of precursor phthalonitrile

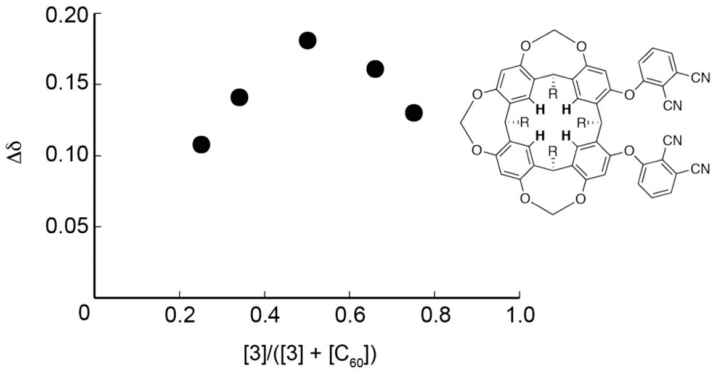

Fig. 1. *Job plot for the chemical shift change of benzene protons* ***H*** *at the lower rim in* ***3*** *+ C_{60} system (^{1}H NMR, $C_6D_5CD_3$, 400 MHz, 298 K).*

Aromatic macrocycles such as *p-tert*-butylcalix[8]arene and *p-tert*-butylcalix[6]-arene can form well-defined supramolecular complexes with fullerenes in solvents.[9-11] The author also expected a supramolecular complex to form between the bridged resorcin[4]arene **3** and C_{60} in solution. The complex formation between **3** and C_{60} was monitored by ^{1}H NMR spectral changes.[25] Upon the addition of C_{60} to a solution of **3** in toluene-d_8, the chemical shift of benzene protons at the lower rim of **3** moved downfield, suggesting the inclusion of C_{60} within the cavity of **3**. A Job plot for the titration study on **3** with C_{60} in ^{1}H NMR spectroscopy confirmed the formation of a 1:1 complex (Fig. 1).[26] The binding constant of **3** with C_{60} was 1100 M^{-1} in toluene-d_8 as inferred from ^{1}H NMR spectroscopic analysis. The cavity in **3** can form a supramolecular complex with C_{60} through C-H $\cdots\pi$ interactions.[9]

4.2.3 Optical property

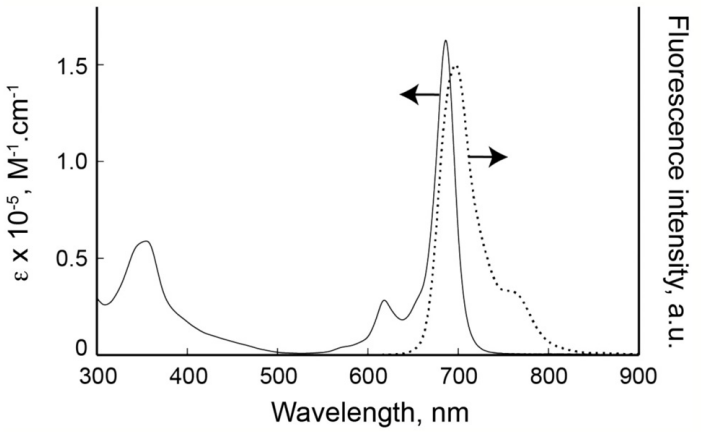

Fig. 2. *Absorption (solid line) and fluorescence spectra (dotted line) of **1** in THF.*

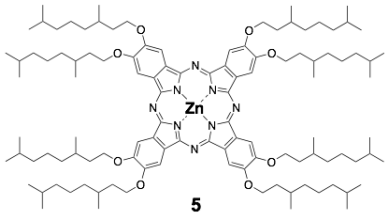

Chart 1 *Structure of **5**: λ_{max} (log ε) = 685 nm (5.20).*

As shown in Fig. 2, the absorption spectrum of **1** in THF showed a sharp and strong peak at λ_{max} = 686 nm and a relatively weak peak at λ_{max} = 365 nm as the Q band and the Soret band of ZnPcs.[27] The absorption spectra of **1** did not change within the concentration range of 3.0×10^{-6} to 1.2×10^{-5} mol L^{-1}. The absorption spectrum of **1** in THF is typical nonaggregated ZnPcs, which follow the Beer-Lambert law. Compound **1** fluoresced at 697 nm in degassed THF upon excitation at the Soret band. The absorption and fluorescence spectra of **1** in THF exhibited nearly the same spectrum at the symmetric 2,3,9,10,16,17,23,24-octa-(3',5'-dimethylhexloxy) phthalocyaninatozinc complex **5** lacking the resorcin[4]arene strap (λ_{max} (log ε) = 685 nm (5.20)). From these spectral results, the introduction of resorcin[4]arene does not affect the electronic conditions of ZnPc.[28]

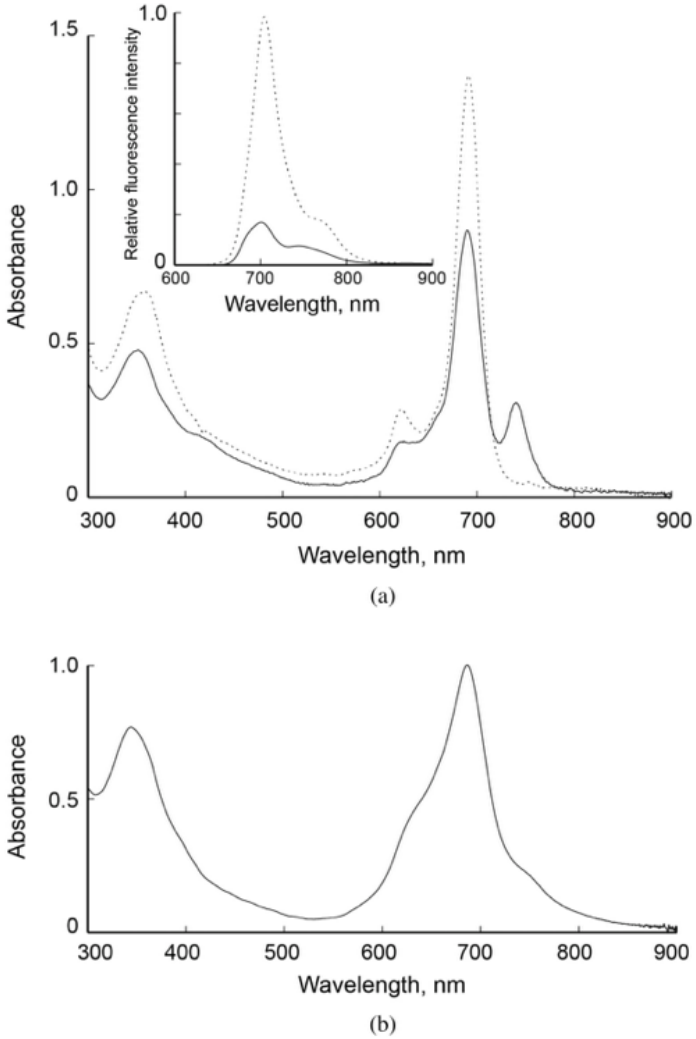

Fig. 3. *a) Absorption spectra of **1** in CH_2Cl_2 (solid line) and CH_2Cl_2+pyridine (0.1 vol%) (dotted line). [**1**] = 5.8 μM. The inset shows the fluorescence spectral change by the addition of pyridine. [**1**] = 1.5 μM. b) Absorption spectrum of **1** in n-hexane. [**1**] = 10.6 μM.*

Fig. 3a shows the absorption and fluorescence spectra of **1** in CH_2Cl_2. While **5** in CH_2Cl_2 displays the same spectrum as that in THF, the Q band of **1** in CH_2Cl_2 splits at 694 and 740 nm. The fluorescence spectrum in CH_2Cl_2 is slightly red-shifted relative to that in THF. The formation of aggregates among MPcs affects the shape and location of the Q band.[29] However, the red shoulder peak of Q band at 740 nm remained unaltered as the concentration of **1** in CH_2Cl_2

decreased, revealing that the appearance of a new shoulder peak of **1** in CH_2Cl_2 was not attributed to the formation of aggregates. The shoulder peak at 740 nm was eliminated, and the solution color was changed from green to blue by adding pyridine to CH_2Cl_2 solution of **1**. Moreover, the fluorescence intensity of **1** was significantly increased by adding pyridine as shown in the inset of Fig. 3a. Micó et al. reported the solvatochromic behavior of unsymmetrical ZnPc possessing a 2-hydroxy-1-naphthylazo moiety.[30] Reddy et al. also reported absorption spectral changes of trifluoroethoxy-substituted ZnPcs with deoxyribonucleosides by light irradiation.[31] These compounds displayed a red shoulder peak of the Q band in CH_2Cl_2 due to the partial protonation on the *meso*-nitrogen of phthalocyanine ligand. The side strapping of one side of phthalocyanine ligand with the resorcin[4]arene macrocycle in **1** stabilizes the protonation of nitrogen close to the strap, and the self-protonation in CH_2Cl_2 results in the appearance of the red shoulder peak of the Q band. The reference ZnPc **5** showed a broad Q band with absorption maximum at 635 nm in *n*-hexane, typical of aggregated MPcs having a cofacial arrangement through π-π interactions. Although the Q band of **1** was slightly broadened in *n*-hexane, **1** showed the same position of Q band at 686 nm as that in THF (Fig. 3b). Introducing bulky resorcin[4]arene prevents the cofacial stacking of ZnPcs.

4.3.4 Host material properties

Since the resorcin[4]arene moiety in **1** can interact with C_{60}, the author expected a photoinduced electron transfer from ZnPc to C_{60} incorporated within the cavity of resorcin[4]arene.[32] The Q band of ZnPc showed no changes after the addition of a large excess of C_{60} in toluene, indicating a negligible interaction between ZnPc and C_{60}. The fluorescence of **1** decreased in intensity upon the titration with C_{60}, and the Stern-Volmer plots of **1** showed a highly efficient fluorescence quenching at a low concentration of C_{60} as compared with **5** (Fig. 4). The larger slope of the Stern-Volmer plot for **1** suggests the static quenching through the complexation of the fluorophore and quencher.

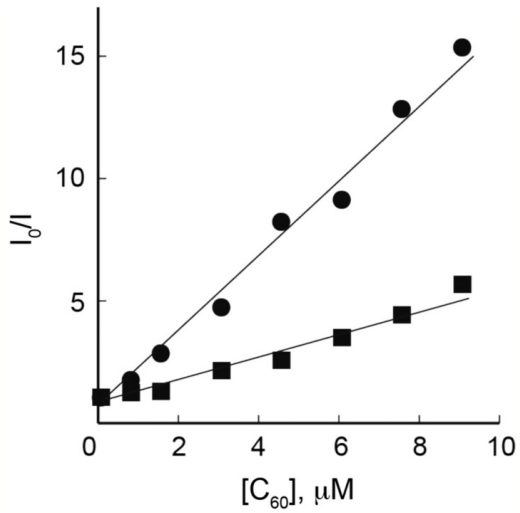

Fig. 4. *Stern–Volmer plots for fluorescence quenching of* ***1*** *(●) and* ***5*** *(■) with* C_{60} *in degassed toluene solution. The fluorescence intensity was monitored at 705 nm upon exciting at 353 nm.* ***[1, 5]*** *= 1.5 μM*

4.4 Conclusion

In summary, the author has synthesized a resorcin[4]arene-strapped zinc phthalocyanine **1** from two phthalonitriles **3** and **4**. Two benzene rings on one side of phthalocyanine ligand were strapped with resorcin[4]arene, and the other two benzene rings were decorated with four branched alkoxy chains. Introduction of resorcin[4]arene strongly affects the spectroscopic property of the phthalocyanine. The shapes and positions of absorption spectra of **1** depend strongly on the nature of solvents. The Q band of **1** in CH_2Cl_2 is split into 694 and 740 nm due to the self-protonation of **1** on the *meso*-nitrogen of phthalocyanine ligand. Bowl-shaped resorcin[4]arene can capture C_{60} through the non-covalent interactions, and the complexation between **1** and C_{60} leads to an efficient electron transfer. Further investigation of photophysical properties of the supramolecular complex of **1** with C_{60} is now underway in our group.

4.5 References

1. Wasielewski MR. *Chem. Rev*. 1992; **92**: 435.
2. Meyer GJ. *Molecular Level Artificial Photosynthetic Materials* in *Progress in Inorganic Chemistry*, Vol. 44, Karlin KD. (Ed.) John Wiley & Sons, Inc.: New York, 1997.
3. Imahori H, Guldi DM, Tamaki K, Yoshica Y, Luo C, Sakata Y and Fukuzumi S. *J. Am. Chem. Soc*. 2001; **123**: 6617.
4. Fukuzumi S, Ohkubo K, Imahori H, Shao J, Qu Z, Zheng G, Chen Y, Pandey RK, Fujitsuka M, Ito O and Kadish KM. *J. Am. Chem. Soc*. 2001; **123**: 10676.
5. Wu, ZQ, Shao XB, Li C, Hou JL, Jiang XK and Li ZT. *J. Am. Chem. Soc*. 2005; **127**: 17460.
6. Yamamoto M, Takano Y, Matano Y, Stranius K, Tkachenko NV, Lemmetyinen H and Imahori H. *J. Phys. Chem. C*, 2014; **118**: 1808.

7. Káš M, Lang K, Stibor I and Lhoták P. *Tetrahedron Lett*. 2007; **48**: 477.
8. Lehtivuori H, Kumpulainen T, Efimox A, Lemm- etyinen H, Kira A, Imahori H and Tkachenko NV. *J. Phys. Chem. C* 2008; **112**: 9896.
9. Ikeda A and Shinkai S. *Chem. Rev*. 1997; **97**: 1713.
10. Huerta E, Pérez EM, Bo C, Martín N and de Mendoza J. *J. Am. Chem. Soc*. 2010; **132**: 5351.
11. Davis CM, Lim JM, Larsen KR, Kim DS, Sung YM, Lyons DM, Lynch VM, Nielsen KA, Jeppesen JO, Kim D, Park JS and Sessler JL. *J. Am. Chem. Soc*. 2014; **136**: 10410.
12. O'Malley S, Schazmann B, Diamond D and Nolan K. *Tetrahedron Lett*. 2007; **48**: 9003.
13. Kantar C, Agar E and Sasmaz S. *Dyes Pigm*. 2008; **77**: 487.
14. Bezzu, CG, Hellowell M, Kariuki BM and McKeown NB. *J. Porphyrins Phthalocyanines* 2011; **15**: 686.
15. Topkaya D, Dumoulin F, Ahsen V and Isci Ü. *Dalton Trans*. 2014; **43**: 2032.
16. de la Torre G and Torres T. *J. Porphyrins Phthalocyanines* 2002; **6**: 274.
17. Mack J and Kobayashi N. *Chem. Rev*. 2011; **111**: 281.
18. Nemykin VN, Dudkin SV, Dumoulin F, Hirel C, Gürek AG and Ahsen V. *ARKIVOC*, 2014; **i**: 142.
19. Leznoff CC and Drew DM. *Can. J. Chem*. 1996; **74**: 307.
20. Kobayashi N. *Chem. Commun*. 1998; 487.
21. Kobayashi N, Miwa H, Isago H and Tomura T. *Inorg. Chem*. 1999; **38**: 479.
22. Kimura M, Ueki H, Ohta K, Shirai H and Kobayashi N. *Langmuir* 2006; **22**: 5051.
23. Tunstad LM, Trucker JA, Dalcanale E, Weiser J, Bryant JA, Sherman JC, Helgeson RC, Knobler CB and Cram DJ. *J. Org. Chem*. 1989; **54**: 1305.
24. Menozzi E, Busi M, Ramingo R, Campagnolo M, Geremia S and Dalcamale E. *Chem. Eur. J*. 2005; **11**: 3136.
25. Bhattacharya S, Nayak SK, Chattopadhyay S, Banerjee M and Mukherjee AK. *J. Phys. Chem B* 2003; **107**: 11830.
26. Renny JS, Tomasevich LL, Tallmadge EH and Collum DB. *Angew. Chem. Int. Ed*. 2013; **51**: 2.

27. Stillman MJ and Nyokong T. *Phthalocyanines Properties and Applications*, Vol. 1, Leznoff CC and Lever ABP. (Eds.) VCH: New York, 1989; pp. 135.
28. Lukyanets EA and Nemylin VN. *J. Porphyrins Phthalocyanines* 2010; **14**: 1.
29. Hassan BM, Li H and McKeown NB. *J. Mater. Chem.* 2000; **10**: 39.
30. Micó XA, Vagin SI, Subramanian LR, Ziegler T and Hanack M. *Eur. J. Org. Chem.* 2005; 4328.
31. Reddy MR, Shibata N, Kondo Y, Nakamura S and Toru T. *Angew. Chem. Int. Ed.* 2006; **45**: 8163.
32. González-Rodríguez D and Bottari G. *J. Porphyrins Phthalocyanines* 2009; **13**: 624.
33. Kimura M, Kuroda T, Ohta K, Hanabusa K, Shirai H and Kobayashi N. *Langmuir* 2003; **19**: 4825.

Summary and Conclusions

In this thesis, the author has designed and synthesized thiophene-fused metallophthalocyanine analogues (**Chapter 2**), thiophene-fused zinc naphthalocyanine analogues (**Chapter 3**), and resorcin[4]-strapped zinc phthalocyanine (**Chapter 4**) for investigation of their optical and electronic functions in various states.

In **Chapter 2** thiophene-fused phthalocyanines **1**–**4** were synthesized through ring closing reactions from *o*-chloroethynylbenzene substructures. The self-organizing properties of thiophene-fused phthalocyanines were investigated in solution, at the air-water interface, and in the solid state. The attachment of *n*-hexylphenyl units at α-positions of the fused thiophene rings creates a network structure of nanoscopic fibrous assemblies with excellent long-range stacking through intermacrocycle interactions, which with the additional interaction between peripheral phenyl spacers. Cu-**1** and Cu-**2** acted as a soluble p-channel organic semiconductor, but the field-effect mobility was not high due to the low crystallinity in the solid state. Cu-**4** possessing thiophene spacers was polymerized into the electrochemically active films onto an electrode by the connection of four thiophene terminals through an oxidative coupling reaction.

In **Chapter 3** two structural regioisomers of near-IR light absorbing **ZnTNc$_{exo}$** and **ZnTNc$_{endo}$** decorated with sixteen long alkyl chains were designed and synthesized. The author has elucidated the influence of the molecular structural differences between the two isomers on their self-organizing behavior and photoconductivity. Ring-expanded **ZnTNc$_{exo}$** and **ZnTNc$_{endo}$** assemble into one-dimensional columnar nanostructures over a wide temperature range from

room temperature. TOF experiments have revealed that organized **ZnTNc$_{exo}$** shows a well-balanced ambipolar carrier transport behavior, with carrier mobilities of the order of 10^{-2} cm^2 V^{-1} s^{-1}. Spontaneous alignment of columnar assemblies on substrates is a key issue for improving the carrier mobilities.

In **Chapter 4** a resorcin[4]arene-strapped zinc phthalocyanine **1** was synthesized from two phthalonitriles **3** and **4**. Two benzene rings on one side of phthalocyanine ligand were strapped with resorcin[4]arene, while the other two benzene rings were decorated with four branched alkoxy chains. The introduction of resorcin[4]arene strongly affects the spectroscopic properties of the phthalocyanine. The shapes and positions of the absorption spectra of **1** depend strongly on the nature of the solvents. The Q band of **1** in CH_2Cl_2 is split into 694 and 740 nm due to the self-protonation of **1** on the *meso*-nitrogen of the phthalocyanine ligand. Bowl-shaped resorcin[4]arene can capture C_{60} through non-covalent interactions, and the complexation between **1** and C_{60} leads to an efficient electron transfer.

Publications

Papers

1. Hiroyuki Suzuki, Naoya Yamada, Ken-ichi Nakayama and Mutsumi Kimura, **Self-organized one-dimensional columns of benzo[b]thiophene-fused tetraazaporphyrins**, *J. Porphyrins Phthalocyanines* 2014; **18**: 259-266.
2. Hitomi Momose, Hiroyuki Suzuki and Mutsumi Kimura, **Supramolecular complex formation of resorcin[4]arene-modified zinc phthalocyanine and fullerene**, *J. Porphyrins Phthalocyanines* 2014; **18**: 843-848.
3. Hiroyuki Suzuki, Koki Kawano, Kazuchika Ohta, Yo Shimizu, Nagao Kobayashi and Mutsumi Kimura, **Topological Control of Columnar Stacking Made of Liquid-Crystalline Thiophene-Fused Metallonaphthalocyaniens**, *ChemistryOpen* DOI: 10.1002/open.201500205.

Other paper

1. Mutsumi Kimura, Hirotaka Nomoto, Hiroyuki Suzuki, Takuro Ikeuchi, Hiroyuki Matsuzaki, Takuro N. Murakami, Akihiko Furube, Naruhiko Masaki, Matthew J. Griffith, and Shogo Mori, **Molecular Design Rule of Phthalocyanine Dyes for Highly Efficient Near-IR Performance in Dye-Sensitized Solar Cells**, *Chem. Eur. J*. 2013; **19**; 7496-7502.
2. Hiroyuki Suzuki, Nagao Kobayashi, and Mutsumi Kimura, **Contorted Arene-fused Metallophthalocyanines**, *Asian J. Org. Chem*. DOI: 10.1002/ajoc.201500532.

Presentations on international symposium

1. Hiroyuki Suzuki and Mutsumi Kimura, **Self-organization of thiophene-fused phthalocyanines**, the International Symposium on Fiber Science and Technology 2014 (ISF2014), Tokyo (Japan), September 2014.
2. Hiroyuki Suzuki and Mutsumi Kimura, **Two-dimensional Methallophthalocyanines fused with Polycyclic Aromatic Structures**, Miyagi (Japan), Michinoku International Symposium on Porpyrins, Phthalocyanines and Functional π Molecules (MISPPF), October 2014.

Presentations on symposium

1. Hiroyuki Suzuki and Mutsumi Kimura, **Electronic and Optical Properties of Benzo[*b*]thiophenes-based Phthalocyanine Analogues**, The 62th SPSJ Annual Meeting, Kyoto (Japan), May 2013.
2. Hiroyuki Suzuki and Mutsumi Kimura, **Optica and Electrochemical Properties of New Thiophene-fused Methallophthalocyanines**, The 63th Conference of Japan Society of Coordination Chemistry, Okinawa (Japan), November 2013.
3. Hiroyuki Suzuki and Mutsumi Kimura, **Ring-expanded Methallophthalocyanines having Large π-planar Structures**, The 94th CSJ Annual Meeting, Aichi (Japan), March 2014.
4. Hiroyuki Suzuki, Kenta Ono, Kazuchika Ohta and Mutsumi Kimura, **Self-organization of Ring-fused Phthalocyanines with Benzodithiophene**, The 95th CSJ Annual Meeting, Chiba (Japan), March 2015.

Acknowledgement

Firstly, the author would like to express his deepest gratitude to his supervisor Prof. Mutsumi Kimura, for his limitless patience, understanding and honest support. Without his guidance and persistent help this dissertation would not have been possible.

Advice and comments given by Prof. Nagao Kobayashi and Mr. Tadashi Fukawa have been a great help in his research. The author is particularly grateful for the assistance given by Dr. Yoshie Shinohara, Junko Takizawa, and Seiko Uda. Many thanks to former members of Satoshi Ohtsuji, Masayoshi Karasawa, Mei Yokokawa, Keisuke Takemoto, and Hiroki Yamagiwa for their suggestions and advises. The author would also like to thank Satoshi Yamamoto, Takuro Ikeuchi, and other members of Kimura Laboratory for the help and moral support.

Finally, the author is greatly indebted to his parents Naoji Suzuki and Toshiko Suzuki for their moral support and warm encouragements.

-March 2016-

Hiroyuki Suzuki